Engineering Geology 352 (2025) 108091

Contents lists available at ScienceDirect

Engineering Geology

journal homepage: www.elsevier.com/locate/enggeo

Physical vulnerability assessment procedures for confined and unconfined (unreinforced) clay brick masonry buildings due to mass movements, rigid foundation

Alfer L. Silva-Ceron *, Jorge A. Prieto, Marco F. Gamboa

EAFIT University, Medellín, Colombia

ARTICLE INFO

Keywords:
Mass movements
Fragility curves
Physical vulnerability
Hazard intensity
Structural damage thresholds
Masonry buildings
Risk assessment
Unreinforced masonry (URM)
Confined masonry (CM)

ABSTRACT

While climate change and urban development in mountainous terrain continue to impact society through geo-mass transport phenomena, quantitative risk models must evolve and be communicated as clearly as possible to enhance the social appropriation of knowledge. Recent advancements in mass movement risk analysis equate external hazard intensity measures with the internal strength of buildings. However, procedures for estimating building capacity and developing fragility curves remain less well-defined, particularly for masonry buildings, which are among the most common construction types worldwide, especially in less developed regions, and where laboratory or field data may be scarce. Fragility curves relate hazard intensity to the probability of reaching or exceeding a level of physical damage and have thus become essential tools in vulnerability and risk assessments related to natural hazards. This paper presents a procedure for deriving structural damage thresholds through fragility curves for mass movements, featuring the following characteristics: it is not based on seismic design parameters, does not require excessive computational resources, and is straightforward to implement. Recognizing that damage during a mass movement event may depend not only on the structural strength of buildings —assuming a rigid foundation— but also on ground resistance, which can cause permanent deformations, this study focuses on the rigid, fixed foundation scenario. The method incorporates geometrical and mechanical parameters along with their associated uncertainties, and provides damage state thresholds as functions of momentum flux and mass movement height for two typical wall types: unconfined, unreinforced clay brick masonry (URM) and confined clay brick masonry (CM).

1. Introduction

Downslope movements of rock mass, debris, or soil due to gravitational influence —commonly referred to as *mass movements* (Cruden, 1991; Hungr et al., 2014)— represent a globally significant natural hazard. In recent decades, both economic and human losses associated with mass movements have increased dramatically and are occurring more frequently (Aristizábal and Sánchez, 2020; Cabral et al., 2023; Chen and Lee, 2004; Corominas et al., 2014; Highland and Bobrowsky, 2008; Huang et al., 2023b; Santi et al., 2011). These catastrophic events result from a combination of factors including population growth, urban and rural development in mountainous regions prone to mass movements, informal construction practices, inadequate natural resource management, and strong triggers such as unusually high rainfall driven by climate change, tectonic activity, and volcanic eruptions. Given this scenario, robust assessment of hazard, vulnerability, and risk associated with mass movements is vital to design and implement effective mitigation strategies (Corominas et al., 2014). However, physical vulnerability assessment —defined as the susceptibility of exposed infrastructure to damage under a given intensity— presents unique challenges in the context of mass movements. The complexity of the phenomenon (e.g., its diverse types and rheological behaviour) and its interaction with built structures have caused research in this area to progress more slowly than in other natural hazard domains, such as earthquake engineering.

Historically, physical vulnerability to mass movements has been addressed through various approaches, each with distinct strengths and limitations. Empirical methods, based on statistical analysis of observed damage and losses following real events (Bell and Glade, 2004; Chen et al., 2021; Du et al., 2013; Eidsvig et al., 2014; Fuchs et al., 2007; Fuchs

* Corresponding author.
E-mail addresses: alsilvac@eafit.edu.co (A.L. Silva-Ceron), jprieto7@eafit.edu.co (J.A. Prieto), mgamboa@eafit.edu.co (M.F. Gamboa).

https://doi.org/10.1016/j.enggeo.2025.108091
Received 17 May 2024; Received in revised form 20 April 2025; Accepted 21 April 2025
Available online 23 April 2025

et al., 2019a; Hu et al., 2012; Kang and Kim, 2016; Liu et al., 2002; Liu and Lei, 2003; Mazzorana et al., 2014; Michael-Leiba et al., 2012; Papathoma-Köhle et al., 2014, 2017; Sterlacchini et al., 2007; Zhang et al., 2018), offer valuable insights rooted in real-world data. However, they often suffer from data scarcity, limited transferability across regions or construction typologies, and insufficient explanation of the structural failure mechanisms—i.e., they may not adequately link structural damage states to hazard intensity (Fuchs et al., 2019a; Hu et al., 2012; Mazzorana et al., 2014; Papathoma-Köhle et al., 2011, 2017).

Some researchers have refined empirical approaches by incorporating detailed local data to develop vulnerability matrices, curves, and indices (Eidsvig et al., 2014; Fuchs et al., 2019b; Papathoma-Köhle et al., 2017, 2022). However, these efforts often overlook structural damage mechanisms caused by flow-structure interaction, which are essential for robust quantitative risk analysis. Experimental approaches, such as small-scale laboratory studies (Sturm et al., 2018a, 2018b), contribute significantly to understanding flow-structure interactions and validating numerical models. Yet, scale effects and the difficulty in representing the heterogeneity of real-world buildings limit their generalizability. Analytical and numerical approaches (Fang et al., 2021; Feng et al., 2019; Luo et al., 2020; Mavrouli et al., 2014; Mavrouli and Corominas, 2010; Zeng et al., 2015) simulate structural responses and offer potential for generalized insights into failure mechanisms. Nonetheless, they often focus on specific building types (e.g., reinforced concrete frames), rely on seismic design parameters that may not be suitable for mass movement loading (Haugen and Kaynia, 2008; Kean et al., 2019; Prieto et al., 2018a), or require computationally intensive simulations (Luo et al., 2019b; Pu et al., 2023), which limits their applicability in practice.

It is important to recognize that empirical, experimental, and analytical approaches are fundamentally complementary. A comprehensive understanding often requires integration of these perspectives; for example, probabilistic damage state estimates are essential for calculating socioeconomic impacts and can be validated with empirical loss data to produce robust quantitative risk assessments (Thouret et al., 2020).

From this review, a clear and significant research gap emerges: the need for a practical, computationally efficient, and physically grounded methodology to assess the vulnerability of unreinforced (URM) and confined (CM) clay masonry buildings to mass movements. These construction types —particularly prevalent in developing countries (Villar-Vega et al., 2017)— have received relatively little attention in the literature. The required methodology should derive structural damage thresholds (preferably in the form of fragility curves) by directly linking relevant flow intensity parameters —such as momentum flux (hv^2) or flow height (h)— to the mechanical response and damage states of masonry walls under lateral loads representative of mass movement events, while avoiding reliance on seismic parameters. Moreover, it should be accessible to practicing engineers, overcoming the cost and complexity barriers associated with sophisticated models, especially in regions with high exposure and limited technical or financial resources.

This article seeks to address this gap by presenting a methodology for assessing the physical vulnerability of URM and CM clay masonry buildings to mass movements, under the assumption of a rigid foundation. The proposed approach employs three-dimensional finite element modelling with a simplified representation of wall nonlinear behaviour (equivalent frame method), incorporates parameter uncertainty via the Rosenblueth point estimation technique (ensuring low computational cost), and derives fragility curves as functions of momentum flux (hv^2) and flow height (h). Probabilistic damage thresholds are developed for buildings with one to four stories and for two common wall thicknesses. The methodology and its results are validated using field data from real events in South Korea and Colombia. This work contributes to the limited body of knowledge on the structural fragility of masonry buildings subjected to mass movements and offers a practical tool for calculating physical vulnerability, ultimately supporting more effective risk assessment and mitigation strategies.

2. Literature review

The literature review, particularly the information summarized in Table 1, reflects the considerable effort that has been devoted to understanding and quantifying the vulnerability of buildings to mass movements. Various approaches have been explored, ranging from empirical analyses based on past events to advanced numerical simulations and experimental studies. However, the review also reveals a series of limitations and recurring gaps that underscore the need for alternative or complementary methodological approaches.

A significant proportion of analytical and numerical studies have focused primarily on reinforced concrete structures (Chen et al., 2021; Luo et al., 2020; Mavrouli et al., 2014; Parisi and Sabella, 2017; Pu et al., 2023), with considerably less attention given to masonry buildings —both unreinforced (URM) and confined (CM)— despite their predominance in many high-risk regions around the world. In some cases, researchers have attempted to model structural capacity using concepts or parameters adapted from earthquake engineering (Haugen and Kaynia, 2008; Kean et al., 2019; Prieto et al., 2018b). While useful as an approximation, these adaptations may not adequately capture the failure mechanisms specific to the loads imposed by mass movements.

Methods relying solely on post-event empirical data, although valuable, face challenges in terms of result transferability to other regions or structural typologies. They also tend to lack insight into the underlying mechanisms of structural failure (Fuchs et al., 2019a; Hu et al., 2012; Papathoma-Köhle et al., 2011). Moreover, high-fidelity numerical simulations and detailed probabilistic analyses often demand substantial computational resources, limiting their widespread application in everyday engineering practice (Luo et al., 2019b; Pu et al., 2023). Finally, many analytical studies simplify the structural-ground interaction by assuming a rigid foundation (Table 1), which may not represent actual conditions.

In response to these identified gaps, the methodology proposed in Section 3 of this article has been specifically designed to offer a novel and practical contribution. First, it addresses the typological gap by focusing explicitly on the vulnerability of URM and CM masonry buildings. Second, it avoids reliance on seismic parameters, instead employing a mechanistic structural analysis tailored to masonry-specific failure modes. Third, it moves beyond the limitations of empirical approaches by deriving physically based fragility functions that offer clearer insight into failure mechanisms and improved potential for generalization. Fourth, it mitigates issues of computational cost and complexity by incorporating efficient techniques such as a simplified equivalent frame model and the Rosenblueth point estimation method. Finally, it provides actionable tools for practitioners, generating fragility curves that directly relate flow intensity parameters (hv^2 and h) to defined structural damage states.

Although the implementation presented in this work assumes a rigid foundation —acknowledged as a necessary first step in addressing foundation-related limitations— the overall framework (Fig. 1) explicitly recognizes the importance of incorporating soil-structure interaction in future developments. The methodology described herein is therefore proposed as a practical and technically sound advance in evaluating the physical vulnerability of a critical yet frequently overlooked class of structures.

3. General methodology

Vulnerability is defined as the degree of physical, social, or economic loss experienced by an element or set of elements at risk due to a hazard of a given intensity (EERI Committee, 1986). This study focuses on the physical vulnerability of unreinforced (URM) and confined (CM) masonry buildings subjected to mass movements. Physical vulnerability refers to the ability of infrastructure (e.g., buildings, roads, bridges) to

Table 1
References on the structural vulnerability of buildings to mass movement.

Reference	Input
Walhorn et al. (2005)	Developed a finite element algorithm to determine the structural performance of individual elements impacted by fluid flow, considering parameters related to geometry and flexural capacity only. This study does not include permanent ground deformation (i.e., flexible foundation) and is only valid for rigid foundations.
Haugen and Kaynia (2008)	Present a practical method to predict structural damage caused by debris flows. Using concepts from dynamics and structural performance under seismic loading, the authors applied seismic fragility curves proposed by FEMA (2003). The method was tested using data from a 1998 debris flow event in Sarno, Italy. The model evaluated the vulnerability of six affected structures and compared the results with observed damage states. Inconsistencies were noted in some cases, prompting the authors to recommend further review and comparison of the field data and underlying assumptions with other events. This study does not include permanent ground deformation and is valid only for rigid foundations.
Mavrouli and Corominas (2010)	Present an analytical methodology for evaluating vulnerability and calculating fragility curves for reinforced concrete frame buildings subjected to rock block impacts. This research does not consider permanent ground deformation and is valid only for rigid foundations.
Quan Luna et al. (2011)	Used the FLO-2D model to estimate the intensity of a debris flow event in Selveta, Italy. Intensity measures included flow height, velocity, impact pressure, and viscosity, used as independent variables. Economic vulnerability was calculated based on the ratio of repair cost to property value. Vulnerability curves were derived through statistical analysis and compared with those from previous studies.
Papathoma-Köhle et al. (2011)	Identify the limitations of empirical vulnerability functions, particularly their restricted applicability to different building types or geographic contexts. Furthermore, these methods do not account for structural damage mechanisms, which limits their usefulness in planning for buildings exposed to mass movement hazards.
Hu et al. (2012)	Assert that most studies have focused on empirical relationships between hazard magnitude and the resulting degree of loss. These empirical vulnerability functions typically overlook key characteristics of at-risk buildings, such as geometry, design, and geographic location. Using field surveys and remote sensing, the authors analyse the characteristics and damage patterns of buildings affected by a mass movement event in Zhouqu, China. They conclude that structural systems based on reinforced concrete frames sustained less damage than those constructed with concrete masonry. The study categorizes damage into five levels: complete, extensive, moderate, light, and very light.
Du et al. (2013)	In a study similar to Li et al. (2010), the authors estimate vulnerability using parameters such as construction materials, element susceptibility, building height and age, foundation and slip depth, and hazard intensity. However, they note that many of these parameters remain subjective and empirical. As such, they recommend gradual calibration and documentation through objective data, expert judgment, and accumulated observations. In addition to structural aspects, the study also includes an assessment of the occupants' vulnerability within the buildings.
Mazzorana et al. (2014)	Propose a methodological and computational framework —combining matrix and finite element methods— for scenario development that accounts for mudflow-structure interaction. Initially, the time-varying impact spectrum is quantified using a two-dimensional debris flow simulation (TRENT 2-D moving bed) and existing empirical formulations. Structural performance, including damage mechanisms, is then evaluated using the SISMICAD 12.1 software. The study adopts two Eurocode damage limit states: the ultimate limit state (beyond which collapse occurs) and the serviceability limit state (up to which functionality is maintained). A third, the material intrusion limit state, considers the ingress of mud or moisture through openings such as doors and windows. The resulting damage susceptibility profile is proposed as a basis for designing effective structural protection. This study does not consider permanent ground deformation and is only applicable to rigid foundations.
Mavrouli et al. (2014)	Present an analytical methodology for assessing vulnerability and developing fragility curves for reinforced concrete frame buildings subjected to landslides. The analysis is based on single-bay, one-storey RC frames and explores variations in physical and mechanical parameters, including the potential presence of weak or flexible foundations (e.g., isolated footings). However, the procedure is not designed for conditions involving ground deformations. The study emphasises the importance of accounting for potential foundation failures when buildings are impacted by mass movements and is proposed as a preliminary step toward more generalizable approaches. The authors highlight the scarcity of studies on structural vulnerability in unstable or sliding slope conditions and advocate for greater research in this area.
Eidsvig et al. (2014)	Propose two methodologies for assessing building vulnerability to debris flows. Both approaches use S-shaped cumulative distribution functions, fitted to empirical data from the Martell Valley event in South Tyrol, Italy, in August 1987. The first model produces vulnerability curves, while the second develops fragility curves based on debris flow height as the intensity measure. The authors state that the methodology is replicable in other regions; however, it depends on the availability of statistically robust data from well-documented past events.
Kang and Kim (2016)	Analysed 11 mass movement events triggered by heavy rainfall in southern Korea during July and August 2011. Flow characteristics —such as height, velocity, and impact pressure— were measured for 25 affected buildings, each of which was classified according to its damage state (slight, moderate, extensive, and complete). The study used field surveys, spatial data, and empirical formulas to analyse the relationship between damage states and mass movement intensity. Three empirical vulnerability curves were derived as functions of flow depth, velocity, and impact pressure. A non-linear regression analysis was performed using an S-shaped sigmoid function, which asymptotically relates vulnerability from near-zero values to a finite upper limit.
Papathoma-Köhle et al. (2017)	Present, compare, and discuss the strengths and limitations of various methods for assessing physical vulnerability to mass movements, including vulnerability matrices, curves, and indices. The authors recommend that future research integrate these three approaches to develop a more comprehensive assessment tool. They also emphasise the importance of incorporating factors such as built environment resilience, laboratory testing, flow-structure interaction, and systematic damage documentation to improve the quality of vulnerability databases.
Parisi and Sabella (2017)	Conducted a fragility analysis of reinforced concrete buildings using flow velocity as the intensity measure. The authors proposed distinct damage states and applied different mechanical models to beams, columns, and infill walls through two-dimensional analysis. They emphasise that seismic design plays a crucial role in mitigating structural fragility caused by mass movements. The analysis considered two-storey, double-bay, two-dimensional reinforced concrete

(continued on next page)

Table 1 (*continued*)

Reference	Input
	frames, treated as subsystems extracted from the full three-dimensional building structure. These frames were assumed to be fixed at the foundation level on an immovable and rigid ground (i.e., no soil–foundation–structure interaction effects were considered).
Zhang et al. (2018)	Present a database derived from a catastrophic mass movement that occurred in August 2010 in Zhouqu County, Gansu Province, Northwest China, which damaged over 390 buildings, including 116 reinforced concrete frames and 274 brick-concrete structures. Using tools such as FLOW-2D, photo interpretation, and field visits, the authors correlate hazard intensity with observed building damage. They propose several empirical models of physical vulnerability curves for damage assessment. However, the database lacks information on specific structural damage states.
Sturm et al. (2018a, 2018b)	Developed an experimental physical model at a 1:30 scale to simulate the 2005 flood event in Schnannerbach, Austria. The impact dynamics of the flow were tested on three buildings. The resulting measurements were used to validate a 3D numerical model (FLOW-3D), incorporating real-time monitoring and multivariable regression. The study establishes correlations between flow intensity and the resulting stresses on structural elements.
Cheung et al. (2018)	Used the LS-DYNA finite element software to numerically simulate the interaction between mass movements and flexible barriers, incorporating non-linear behaviour. The coupled analysis enabled a detailed investigation of the energy balance involved in the impact process.
Prieto et al. (2018b)	Present a methodology that links hazard intensity to the probability of structural damage through the use of fragility functions. These functions estimate the likelihood of exceeding predefined damage states as a function of debris flow intensity, in accordance with FEMA guidelines (2012, 2017; FEMA P-58, 2012). The study includes detailed damage thresholds for URM structures in Medellín, Colombia, with fragility curves expressed in terms of momentum flux. The results were compared with field data from debris flow events that occurred in July and August 2011 in South Korea (Kang and Kim, 2016). This research assumes a rigid foundation and does not account for permanent ground deformation (i.e., flexible foundation).
Papathoma-Köhle et al. (2019)	Introduce a method for calculating Physical Vulnerability Indices (PVI) for floods in the European Alps. Each characteristic of the physical environment is evaluated as a weighted contribution, based on expert input and field observations. The final index is derived from the sum of indicators —such as vulnerability to mass movement intrusion, exposure, and building characteristics— each adjusted by its assigned weight. According to the authors, PVIs offer the advantage of providing detailed information on specific environmental parameters, representing an alternative approach to assessing physical vulnerability. However, this method does not consider structural damage mechanisms resulting from interaction with mass movements.
Luo et al. (2019a)	Simulate the mass movement that occurred on December 20, 2015, in Shenzhen, China, using three-dimensional terrain modelling with the explicit integration software LS-DYNA. The study examines three scenarios: green field (no structures), moving buildings (to simulate ground sliding), and fixed buildings. The simulations demonstrate that the presence of densely distributed buildings significantly influences flow patterns, displacement distance, deposition zones, and the energy transfer mechanism. The case involving moving buildings more accurately represents real flow conditions, as fixed buildings impose greater constraints on the moving mass, resulting in increased deformation, higher internal energy, and lower kinetic energy of the soil. The largest dissipation of frictional energy is observed in the mobile building scenario due to the long sliding distances of damaged structures. The findings emphasise the importance of considering clusters of buildings when conducting hazard mapping and risk assessments for mass movement scenarios.
Feng et al. (2019)	Propose a numerical method to simulate debris flow and its interaction with buildings over three-dimensional terrain, accounting for the destruction process. The method uses smoothed particle hydrodynamics (SPH) to model the flow and finite element methods (FEM) to represent the structural components of buildings.
Fuchs et al. (2019b)	Indicate that recent advances in vulnerability assessment methods for buildings exposed to torrential hazards evidence significant research gaps. The authors highlight that, despite numerous studies on the physical vulnerability of buildings, there is still limited understanding of the interaction between structures and the triggering hazard events.
Kean et al. (2019)	Document and map the 2018 Montecito debris flow event in California, USA, which affected several buildings. Hazard intensity was quantified in terms of height, velocity, and momentum flux. Fragility was assessed using the methodology proposed by Prieto et al. (2018a), resulting in threshold classifications of light, moderate, extensive, and complete structural damage for wooden buildings. Fragility curves were developed based on momentum flux and debris flow height. This study does not account for permanent ground deformation (i.e., flexible foundations) and is valid only for rigid foundation scenarios.
Liang and Xiong (2019)	Investigate the vulnerability of bridge structures in China subjected to mass flows by developing a two-dimensional structural model—a transverse frame of two reinforced concrete columns. The impact forces of debris flows were applied in the frame's plane. Deformations were computed using nonlinear pushover analysis in the CSI-Bridge software. Based on evaluation indices and damage exceedance probabilities, fragility curves were derived and compared with findings from other authors. This study assumes rigid foundations and does not incorporate permanent ground deformation.
(Luo, Zhang, et al., 2019) (Luo et al., 2020)	Address a critical gap in mass movement risk analysis: the evaluation of structural response and vulnerability. The study focuses on reinforced concrete frame-type buildings subjected to debris flow impacts, using explicit time integration via the LS-DYNA software. A five-class damage classification system was developed, based on field observations and simulation results. The authors argue that relying on a single intensity measure (e.g., impact pressure) is insufficient for predicting damage levels. They suggest that buildings in which both structural and non-structural components survive the initial impact are more likely to reach a stable state, due to the rapid decrease in impact pressure. The study concludes that structural capacity against landslides primarily depends on the global lateral resistance of the building, although local failures —particularly in columns and walls perpendicular to the flow— are also possible. Notably, the analyses are deterministic; a fragility analysis that incorporates uncertainties related to hazard and building properties has not been performed due to computational limitations. The method used is nonetheless considered valuable for identifying key factors in vulnerability, supporting the development of fragility functions and reliability-based models. The foundation is not modelled; instead, fixed boundary conditions are applied to the base nodes of columns and walls, meaning that only the superstructure is subjected to mass movement impacts.
Luo et al. (2020)	This study incorporates the interaction between hazard intensity, structural damage mechanisms, and uncertainty in implicit variables using OPENSEES software and Monte Carlo simulation. Fragility curves

(*continued on next page*)

Table 1 (*continued*)

Reference	Input
	for reinforced concrete frame buildings are developed. The authors emphasise that the selection of intensity measures should align with specific failure mechanisms, such as force-dominated or moment-dominated behaviour. Composite indicators like impact force (hv^2) and overturning moment (h^2v^2) are used and reflected in the fragility curves. This research assumes a rigid foundation and does not account for permanent ground deformation.
Thouret et al. (2020)	Provide a review of the state of the art in mass movement risk management, emphasizing that damage state probabilities are essential for estimating socioeconomic consequences. These probabilities can be used in conjunction with empirical loss data to produce quantitative risk assessments.
Fang et al. (2021)	Using explicit time integration via LS-DYNA, this study investigates the failure mechanisms and structural response of a typical reinforced masonry building subjected to flood impacts. The analysis assumes a rigid foundation and does not consider permanent ground deformation.
Chen et al. (2021)	Reproduce the debris flow event of August 20, 2019, in Cutou Creek, Wenchuan, Southwest China, using FLOW-2D simulation. The study identifies momentum flux (hv^2) as a realistic indicator of the hydrodynamic forces that lead to lateral building displacement and associated damage. A database of affected buildings and corresponding damage levels was compiled. Based on this data, physical fragility curves were proposed for unreinforced masonry and wood buildings, following the methodology of Eidsvig et al. (2014), offering a scientific basis for improved risk management and mitigation.
Luo et al. (2023)	Summarize recent developments in vulnerability and risk assessment related to mass movements, including progress in multi-hazard vulnerability modelling. The study emphasises that vulnerability assessment within a multi-hazard framework remains an emerging and evolving research field.
Huang et al. (2023a)	Presents a sensitivity analysis of peak impact forces acting on buildings, considering environmental parameters such as the orientation, size of openings, azimuthal angle, and proximity of surrounding structures. Impact forces were derived from a monophasic viscous debris flow using a simplified synthetic hydrograph in FLOW-3D (a computational fluid dynamics model), and validated through physical modelling.
Capparelli et al. (2023)	Calibrate a model using both numerical methods (via ABAQUS) and semi-quantitative techniques, assigning weights and scores to flood exposure and the physical and mechanical properties of URM buildings. Probabilistic analysis was conducted using Monte Carlo simulation to derive hazard and vulnerability indices for flood damage estimation. Structural stability in the model depends exclusively on the out-of-plane behaviour of walls; in-plane capacity is not considered. Collapse is assumed when the first wall or panel fails. The analysis does not include permanent ground deformation.
Chen et al. (2023)	Apply a risk model for different return periods, calculating hazard using FLO-2D and estimating vulnerability via adjusted empirical fragility curves based on observed building damage from a specific event, following Eidsvig et al. (2014). Structural damage levels and associated economic losses were weighted to quantify risk. The study analyses two building types —brick-concrete and masonry-wood— but does not perform physical or mechanical modelling. Instead, vulnerability is inferred from post-event damage records. While useful, the method is not easily generalizable due to its dependence on localized, event-specific data.
Pu et al. (2023)	Conclude that commonly used methods for assessing vulnerability to mass movements —such as Monte Carlo simulation and Latin hypercube sampling— are inadequate due to high computational demands. As an alternative, the authors propose dynamic contact modelling based on the generalized F-discrepancy method (GF-discrepancy), which better captures interactions between hazards and buildings (Chen et al., 2016; Yang et al., 2020). In their study, they derive damage mechanisms, vulnerability metrics, and fragility curves for a two-storey reinforced concrete frame building. The analysis assumes a rigid foundation with full constraints, excluding ground deformation effects.

withstand hazard-related impacts. Two primary types of functions are commonly used to represent this phenomenon: vulnerability curves and fragility curves.

Vulnerability curve functions have typically been employed in regions where data on the economic or social consequences of past events is available. However, reliable data is often scarce, and these curves are difficult to apply retrospectively —even to the same site— because the underlying characteristics of the system can vary significantly. In the context of mass movement vulnerability, these curves are generally constructed by contrasting event intensity with expected economic losses (Papathoma-Köhle et al., 2022; Quan Luna et al., 2011). However, such studies do not account for the structural performance of buildings. As a result, they are unable to predict structural capacity or its uncertainty and cannot be applied in integrated multi-hazard risk analyses (e.g., earthquake, tsunami, Natech scenarios). An alternative approach for deriving loss functions involves expert judgment, in which qualified individuals estimate losses based on their experience and available information. While this method can be valuable, it is also inherently subjective. By contrast, fragility curves provide, for a given intensity level, the probability of reaching or exceeding a specific damage state. These curves are often modelled using cumulative lognormal distributions (FEMA, 2012) and are widely accepted as a reliable measure of a building's resistance to natural hazards. Due to their probabilistic nature, fragility curves inherently account for uncertainty in damage estimation. As such, they are particularly well-suited for multi-hazard risk analysis and are considered essential for assessing physical risk related to natural phenomena, including mass movements.

Given the advantages of fragility curves —especially their capacity to reflect structural performance and support probabilistic risk assessments— this study focuses on developing a methodology to derive fragility curves and associated damage thresholds for URM and CM masonry buildings exposed to mass movements. It is first necessary to recognize that building vulnerability under such events stems from two distinct but related mechanisms: (1) the direct impact of moving masses on the structure, which induces deformations; and (2) permanent ground deformations or failures, which can compromise the foundation. The first scenario can be addressed as a fixed or rigid base structural problem, while the second involves more complex modes of ground–foundation failure. Fig. 1 outlines the general procedure proposed for evaluating building vulnerability, incorporating both effects. However, the focus of this study is on the first case: the structural response under the assumption of a rigid foundation.

4. Physical vulnerability model

Following the proposed methodology, a three-dimensional structural model is considered under the assumption of a rigid foundation—i.e., no deformations are allowed at the base. This simplification facilitates the modelling process by allowing the analysis to focus on the parameters most relevant to the system's structural performance. To understand the overall behaviour of masonry buildings subjected to mass movements, it is important to recognize that the walls parallel to the flow direction

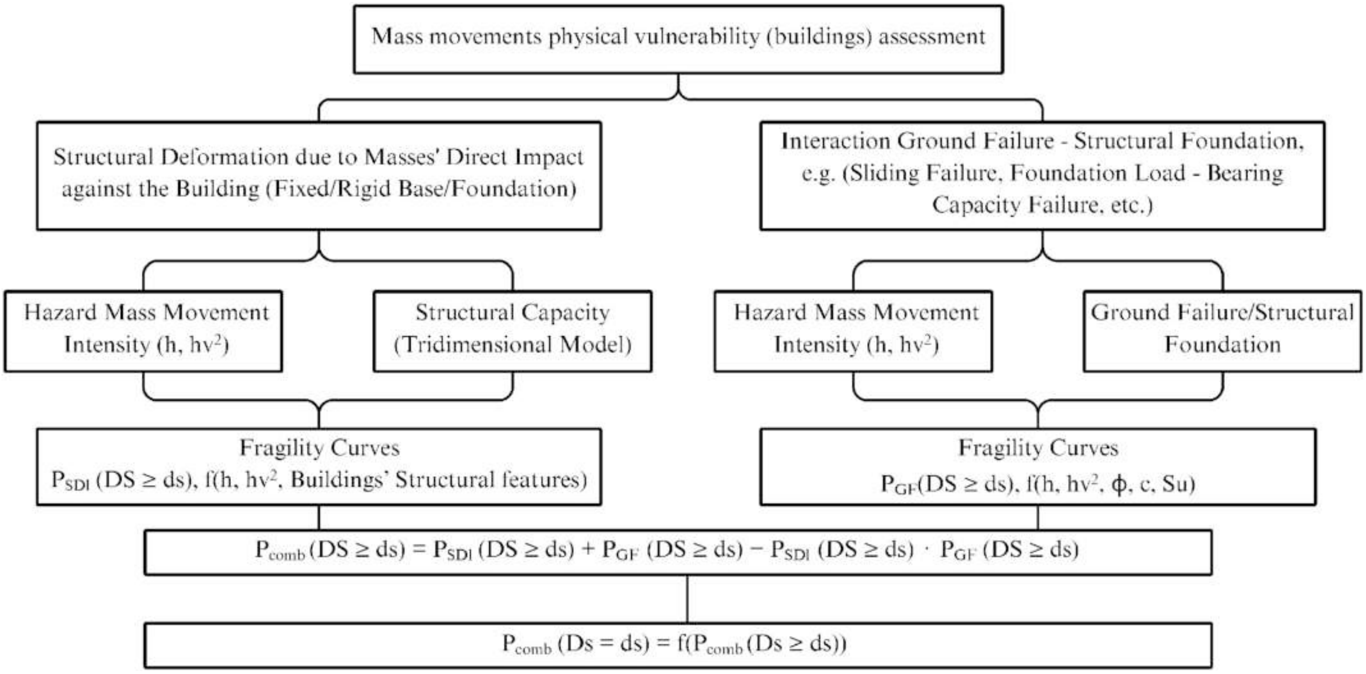

Fig. 1. Methodology for assessing the physical vulnerability of buildings to mass movements. PSDI (DS ≥ ds): Probability of reaching or exceeding a given damage state due to the direct impact of the mass movement on the building. PGF (DS ≥ ds): Probability of reaching or exceeding a damage state due to permanent ground deformation. Pcomb (DS ≥ ds): Combined probability of reaching or exceeding a damage state considering both direct impact and ground deformation. Pcomb (DS = ds): Combined probability of being in a specific damage state resulting from either direct impact or permanent ground deformation. Su: Soil undrained strength; c: Effective cohesion; ϕ: Effective friction angle; h: Mass movement height; hv^2: Momentum flux.

play a key role in resisting the impact, primarily due to their stiffness and strength. The mechanical and probabilistic behaviour of these structural elements is analysed in the following sections.

4.1. Mechanical analysis

The structural response of masonry buildings to external loads —including those generated by mass movements— is governed largely by the shear strength of the walls, particularly in low-rise buildings. This shear capacity can be idealized using non-linear mathematical models that represent each wall as an equivalent structural frame element, following the wide-column method (Borah et al., 2023; Gonzales et al., 2020). In this approach, equivalent frames incorporate a half-height shear hinge that allows lateral deformation. A fixed-base condition is assumed at the bottom of the frame, while an infinitely stiff beam is considered at the top of the wall (Figs. 2 and 3). The shear hinge (modelled as a cutting ball joint) enables the construction of a displacement versus shear force diagram—i.e., the wall's lateral capacity curve. This modelling approach ensures that the structure's kinematic compatibility conditions are satisfied.

Each equivalent frame is then assembled to construct a three-dimensional model of the building. The overall performance of the structure under mass movement loading is evaluated using a nonlinear static analysis procedure based on progressive failure, commonly referred to as the pushover method (Fig. 4). This technique is a powerful tool for assessing the inelastic behaviour of structures subjected to lateral loading (Khan, 2013). The conventional pushover method examines how a structure deforms and ultimately collapses under a monotonically increasing lateral load distribution (Panyakapo, 2014).

With regard to masonry failure modes under lateral loads such as those caused by mass movements, this study emphasises the shear strength behaviour of walls both with and without confinement. The shear capacity of the masonry was analysed considering the effects of compressive stresses induced by gravitational loads acting perpendicular to the horizontal joints.

Unconfined, unreinforced masonry (URM) typically consists of walls constructed with fired clay bricks bonded with lime or cement mortar. This material system is heterogeneous and nonelastic, with brick properties that vary across regions depending on local soil composition and the specific techniques used for molding and firing (Joshi and Jain,

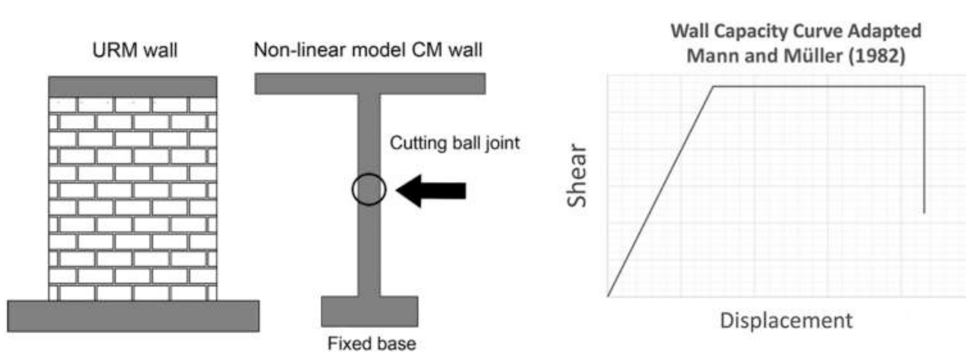

Fig. 2. URM wall and its equivalent nonlinear model.

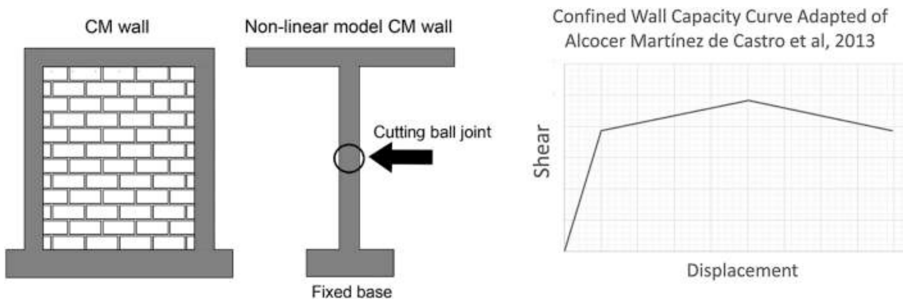

Fig. 3. CM wall and its equivalent nonlinear model.

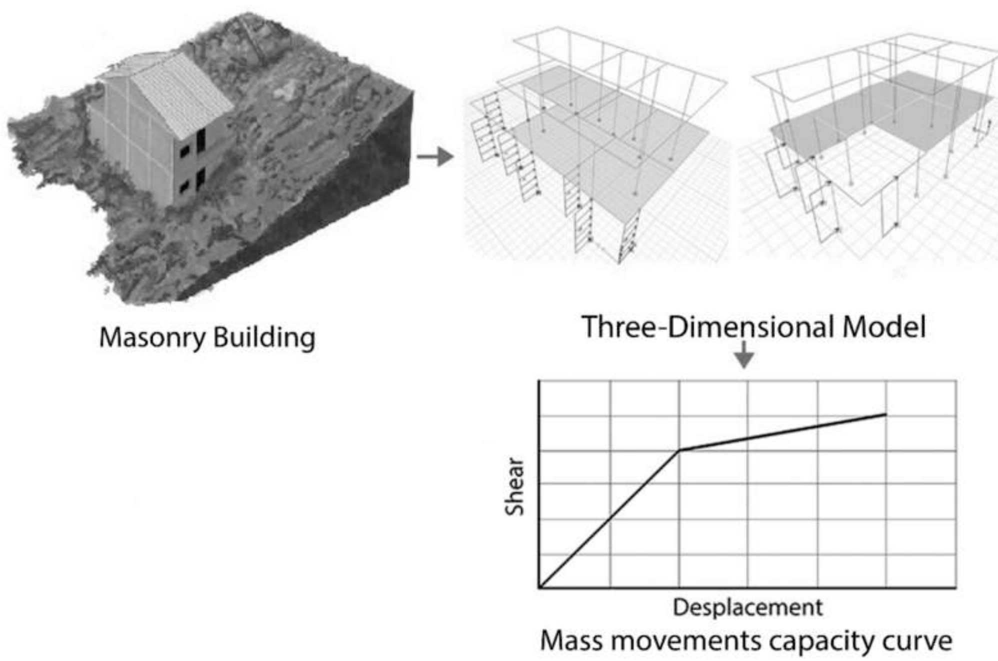

Fig. 4. Conventional pushover analysis and building capacity curve.

2013). The most critical behaviour considered in this study is based on the failure modes proposed by Mann and Müller (1982) (cited in Szabó et al., 2023), which characterize masonry response as brittle in tension due to the bricks and weakened by the presence of mortar joints. Three primary failure modes are considered: friction-shear, diagonal tension, and compression (Figs. 5 and 6). The friction-shear mode occurs under

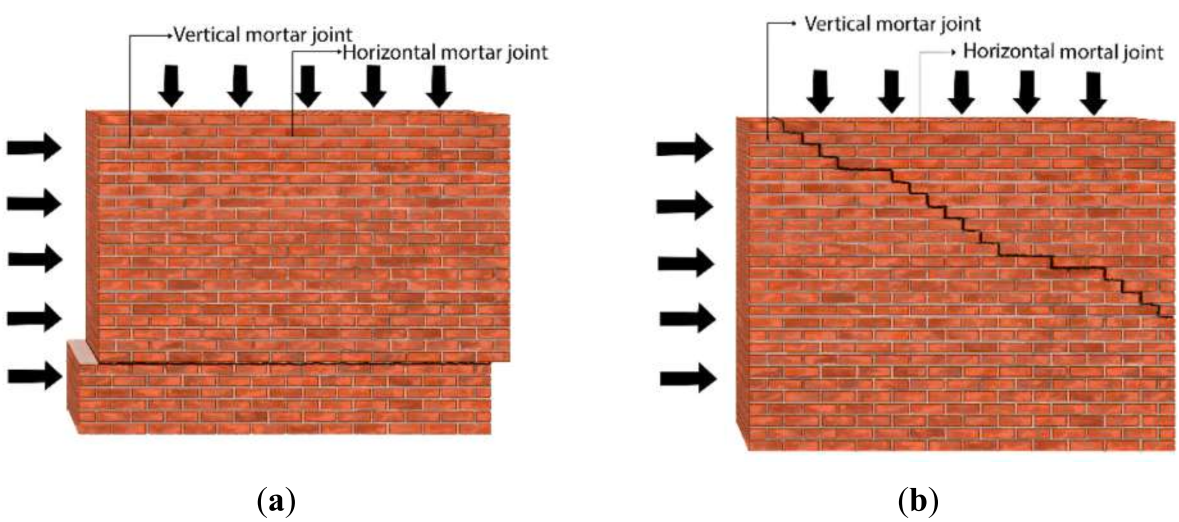

Fig. 5. (a) Friction-shear failure mode: sliding along horizontal joints; (b) Friction-shear failure mode: sliding along horizontal and vertical joints in unreinforced masonry (URM) walls.

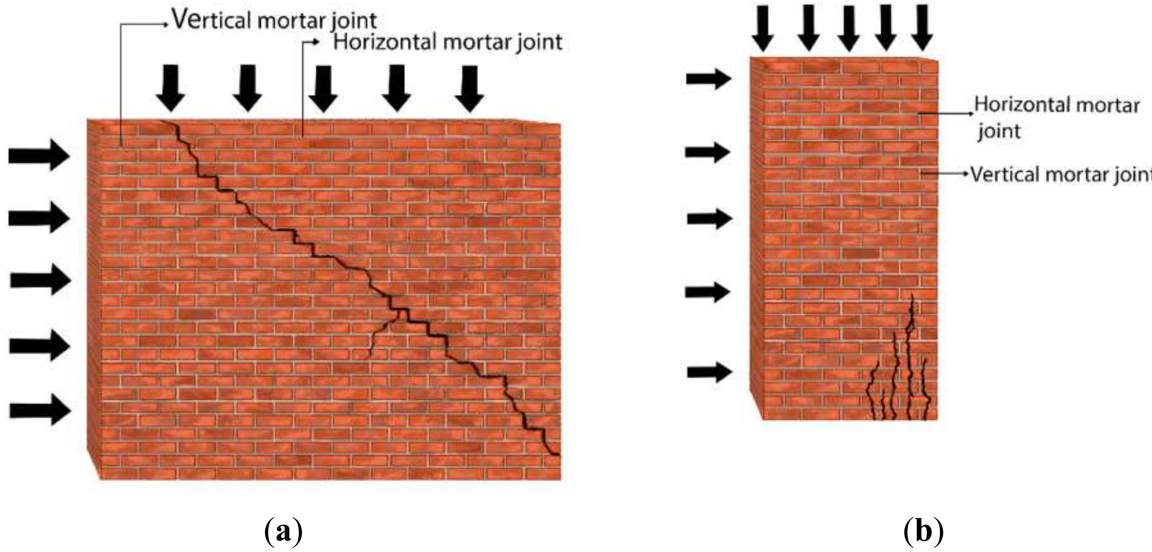

Fig. 6. (a) Diagonal tension failure mode in URM masonry (including cracking of bricks); (b) Compression failure mode in URM masonry.

low compressive normal stress and is primarily associated with weak bonding between mortar and brick, leading to sliding shear failures along the horizontal and vertical joints (Fig. 5). The calculation of shear strength in this mode follows the Mohr-Coulomb failure criterion, adjusted using an empirical coefficient based on experimental data.

$$V_1 = \left(\frac{c + \mu\,\sigma_v}{1 + \mu\frac{2h}{l}}\right) tL \tag{1}$$

Where c is the cohesive strength of the masonry bed joints, $\mu = \tan(\phi)$ is the friction coefficient of the bed joints, ϕ is the friction angle, σ_v represents the gravitational load acting on the wall, and t and L denote the thickness and length of the wall, respectively. h and l refer to the height and length of the individual bricks.

When normal compressive stresses are moderately increased, the shear strength of the mortar joints also increases. Under such conditions, it becomes likely that diagonal tension failure will occur within the brick units of URM walls (Fig. 6a). The shear strength associated with this failure mode is calculated using Eq. (2), where f'tb is the tensile strength of the brick, assumed to be 10 % of its compressive strength f'cb.

$$V_2 = \left[\frac{f'tb}{2.3}\sqrt{\left(1 + \frac{\sigma_v}{f'tb}\right)}\,\right] tL \tag{2}$$

At very high levels of normal stress, failure occurs in compression, resembling the failure mode observed under direct compressive loading. However, in this case, the presence of shear stress leads to a reduction in the masonry's compressive strength (Fig. 6b). The shear strength associated with this failure mode is calculated using Eq. (3), where f'm is the compressive strength of the masonry.

$$V_3 = \left[(f'm - \sigma_v)\frac{l}{2h}\right] tL \tag{3}$$

With regard to deformation calculations, the relationship between shear stresses and the lateral stiffness of the wall enables the estimation of the yield-limit deformation. The wall's stiffness in the elastic range is determined according to Alcocer-Martínez de Castro et al. (2013), as shown in Eq. (4):

$$K_e = \left(\frac{H^3}{\beta E_m I_m} + \frac{\gamma H}{A G_m}\right)^{-1} \tag{4}$$

Where H is the effective height of the wall; E_m is the modulus of elasticity of the masonry; G_m is the masonry shear modulus; A is the effective shear area; β is a coefficient based on wall support conditions: 3 for cantilever walls, 12 for fixed-end walls, 9 is used for intermediate floors, and 3 for top floors with lightweight roofs; I_m is the moment of inertia of the wall section; γ is a shape factor relating average shear stress to maximum shear stress, equal to 1.2 for rectangular sections.

Recognizing that URM walls subjected to lateral loading typically exhibit brittle behaviour, a perfect elastoplastic capacity curve is assumed. The ultimate strain is taken as three times the yield strain, following Fenton (1989).

Confined Masonry (CM) is a construction system where the masonry structural walls are confined on its four sides by reinforced tie columns and tie beams (Adhikari et al., 2023) (Fig. 7). The confining elements have the same thickness as the wall.

CM walls must be properly distributed along both principal directions of the building, in plan and elevation. This configuration provides significantly improved structural performance under lateral loads when compared to unreinforced masonry (URM) buildings.

Statistically calibrated trilinear capacity curves for CM walls —both with and without transverse reinforcement— subjected to lateral loads applied in-plane have been proposed by Flores and Alcocer (1996). Building on this and subsequent experimental work, Alcocer-Martínez de Castro et al. (2013) proposed a trilinear curve for the inelastic range. The cracking shear strength is estimated using Eq. (5). The maximum

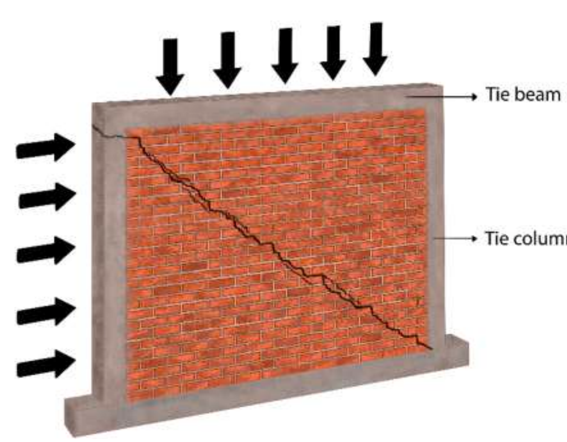

Fig. 7. Diagonal compression failure mode in confined masonry (CM) walls and arrangement of reinforced tie columns and tie beams.

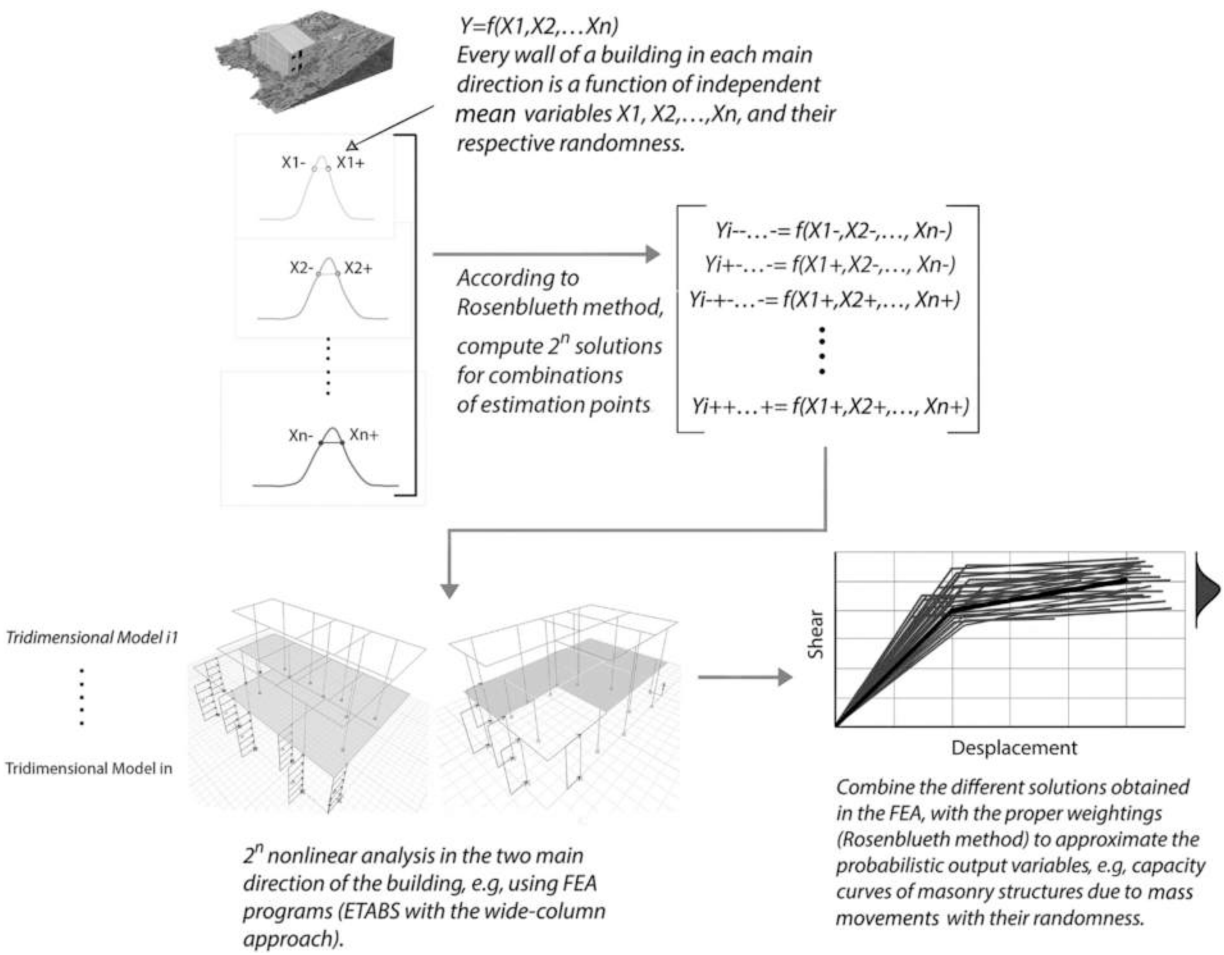

Fig. 8. General procedure for obtaining structural capacity curves using the Rosenblueth point estimation method.

shear strength and ultimate shear strength are determined using Eqs. (6) and (7), respectively.

$$V_{cr} = (0.5v_m + 0.3\sigma_v)tL \leq 1.5v_m tL \quad (5)$$

$$V_{max} = V_{cr} + 1.26\eta n d_b{}^2 \sqrt{f^{\prime}c fy} \leq 1.25V_{cr} \quad (6)$$

$$V_{ult} = 0.8V_{max} \quad (7)$$

Where v_m is the nominal shear stress of the masonry, σ_v is the gravitational load on the wall, t and L are the wall thickness and length, n expresses the number of longitudinal reinforcement bars, η is the efficiency factor (0.3), d_b is the diameter of the longitudinal reinforcement, f'c is the compressive strength of the concrete, and fy is the yield strength of the longitudinal reinforcement. Regarding the calculation of deformations, the relationship between the shear force and the wall's lateral stiffness allows for deducing the yield-limit deformation. The stiffness in the elastic range is determined using Eq. (8), where Ic and Is represent the contributions of the tie columns and longitudinal steel to the total moment of inertia, respectively.

$$K_e = \left[\frac{H^3}{\beta E_m(I_m + I_c + I_s)} + \frac{\gamma H}{AG_m}\right]^{-1} \quad (8)$$

The displacement corresponding to the maximum shear force V_{max} is calculated as the ratio between V_{max} and 25 % of the wall's lateral stiffness (Ke). The displacement corresponding to the ultimate shear force V_{ult} is determined by dividing V_{ult} by 11.25 % of the wall's lateral stiffness (Ke) (Alcocer-Martínez de Castro et al., 2013).

4.2. Probabilistic model

The performance analysis of masonry buildings involves multiple variables, each associated with a certain degree of uncertainty. To capture the variability of these parameters within a three-dimensional model, simulation methods such as the Monte Carlo technique, are typically employed. However, Monte Carlo simulations require a large number of iterations —often in the hundreds of thousands or even millions— to achieve statistically reliable outcomes. This makes the approach computationally expensive and impractical for routine application, especially in resource-constrained settings, typical of many re-

Table 2
Statistical mechanical parameters URM structures.

Parameter	Mean value	sd
f'm (MPa)	3	0.9
c (MPa)	0.14	0.08
μ	0.6	0.3
f'cb (MPa)	5	2

Table 3
Statistical mechanical parameters CM structures.

Parameter	Mean value (MPa)	sd
f'm	3	0.9
νm	0.48	0.05
f'c	20	4
fy	420	25

Table 4
Standard deviations, URM and CM structures.

Parameter	Mean value (MPa)	sd
σ_{v11}	0.065	0.015
$\sigma_{v\ 21}$	0.20	0.050
$\sigma_{v\ 22}$	0.065	0.015
$\sigma_{v\ 31}$	0.38	0.09
$\sigma_{v\ 32}$	0.20	0.050
$\sigma_{v\ 33}$	0.065	0.015
$\sigma_{v\ 41}$	0.49	0.110
$\sigma_{v\ 42}$	0.38	0.09
$\sigma_{v\ 43}$	0.20	0.050
$\sigma_{v\ 44}$	0.065	0.015

Note. σ_{vij} refers to the mean afferent gravitational load acting on a wall in building *i*, located at level *j*. This value includes the self-weight of the wall, slabs, ceiling, roof, and 20 % of the live loads.

Table 5
Identification of variables for URM and CM used in correlation calculations.

Parameters (URM)	ID	Parameters (CM)	ID
f'm	1	vm	1
c	2	f'c	2
μ	3	fy	3
σv	4	σv	4
f'cb	5	f'm	5

gions in the Global South (Asteris et al., 2014; Thinley and Hao, 2017). If there are n variables, and assuming that each variable requires at least 1000 values to define its probability density function (Heijungs, 2020), the total number of combinations becomes 1000^n. For instance, modelling five parameters would require 1000^5 runs of a three-dimensional structural model. In contrast, the point estimation method used in this study would only require $2^n = 32$ runs for five parameters. Therefore, this research adopts the point estimation method for probabilistic moments originally proposed by Rosenblueth (1975), which incorporates both epistemic and aleatory uncertainty in the structural performance model. This method significantly simplifies the estimation of a function's mean and standard deviation, and although its precision may slightly diminish with highly dispersed variables, it remains an efficient and practical alternative (Thinley and Hao, 2017). From the function $Y = f(x_1, x_2, \ldots, x_n)$, where n is the number of variables, it is necessary to define the mean value (μ_{xi}) and standard deviation (σ_{xi}) of each variable x_i. According to the method, there are 2^n combinations of the form $Y_{ij\ldots n} = f(\mu_{xi} \pm \sigma_{xi}, \mu_{xn} \pm \sigma_{xn})$. The expected value and standard deviation of the function are then calculated using Eqs. (9) and (10), respectively:

$$E(Y) = \sum \left(P_{ij..n}\right)\left(Y_{ij..n}\right) \tag{9}$$

$$S(Y) = \sqrt{E\left(Y^2\right) - \left[E(Y)\right]^2} \tag{10}$$

The weighting factor $P_{ij..n}$ for each estimate is defined in Eq. (11):

$$P_{ij..n} = \frac{1}{2^n}\left(1 \pm \sum \rho_{ij..n}\right) \tag{11}$$

The term $\rho_{ij..n}$ denotes the correlation coefficients between the function's variables. The number of correlations among *n* variables is given by the relation $\frac{n(n-1)}{2}$, and 2^n weighting factors are calculated accordingly. A general illustration of Rosenblueth's method is presented in Fig. 8.

The mean mechanical property values and their corresponding standard deviations for URM and CM structures were taken from Tables 2 and 3, while gravitational load conditions are shown in Table 4. These parameters were compiled from several key references (Afanador-García et al., 2012; Ahmed et al., 2019; Flores et al., 2013; Joshi and Jain, 2013; Khanmohammadi et al., 2014; Luo et al., 2021; Magenes and Calvi, 1997; Meli and Reyes, 1971; Muhit et al., 2022; Odacıoğlu and Doğan, 2019; Paulay and Priestley, 1992; Vamvatsikos and Pantazopoulou, 2010). In addition, expert opinion was considered to complement the database. The parameters used are representative of existing masonry buildings, which in many cases are the result of informal construction processes carried out with low-quality standards.

For the probabilistic analysis based on Rosenblueth's method, it is essential to consider the correlations between the involved variables. In general, the correlation between the physical and mechanical properties of masonry depends on multiple factors, including the type of masonry, the characteristics of confinement (if present), the properties of the constituent materials, the conditions of the contact surfaces, surface roughness, curing conditions, the presence of lubricants or slip agents, construction quality, and load conditions, among others. The correlation coefficients used in this study are presented in Table 6. These values are derived from a combination of published references (CEN, 2005; Elghazouli and Peppin, 2011; Gonen et al., 2022; Gumaste et al., 2007; Jafari et al., 2017, 2022; Masonry Standards Joint Committee, 2013; Odacıoğlu and Doğan, 2019; Pulatsu et al., 2020) and expert judgment. For clarity, Table 5 provides the identification of each variable used in the correlation matrix.

4.3. Masonry structures' capacity curves

Three-dimensional models of URM and CM buildings were analysed

Table 6
Correlation coefficients for URM and CM walls used in the application of Rosenblueth's method.

Correlation (URM walls)	ID	Correlation (CM walls)	ID
1_2	0.3–0.5	1_2	0
1_3	0.1–0.2	1_3	0
1_4	0.3–0.5	1_4	0.3–0.5
1_5	0.3–0.5	1_5	0.3–0.5
2_3	0.0–0.2	2_3	0
2_4	0	2_4	0
2_5	0	2_5	0
3_4	0	3_4	0
3_5	0	3_5	0
4_5	0	4_5	0.3–0.5

Table 7
Capacity curve results for masonry structures with 12 cm wall thickness.

Structure Group	Median value		β
	Fy (kN)	Fu (kN)	sdln
URM 1 Storey	102	114	0.41
URM 2 Storeys	189	221	0.36
URM 3 Storeys	302	333	0.31
URM 4 Storeys	352	386	0.31
CM 1 Storey	246	340	0.10
CM 2 Storeys	441	583	0.10
CM 3 Storeys	746	1004	0.10
CM 4 Storeys	868	1126	0.13

Table 8
Capacity curve results for masonry structures with 20 cm wall thickness.

Structure Group	Median value		β
	Fy (kN)	Fu (kN)	sdln
URM 1 Storey	166	206	0.45
URM 2 Storeys	285	337	0.37
URM 3 Storeys	411	461	0.31
URM 4 Storeys	547	602	0.27
CM 1 Storey	444	681	0.10
CM 2 Storeys	741	1040	0.10
CM 3 Storeys	1323	1780	0.10
CM 4 Storeys	1571	2004	0.13

Table 9
Log-normal distribution parameters used to construct the fragility curve for URM buildings (complete damage state). Based on Prieto et al. (2018a).

Parameter	Median value	β (sdln)
K_d	1.2	0.52
ρ (kg/m^3)	2000	0.12
C_d	2	0.37
W (N)	812,793	0.60
B (m)	7.1	0.24
W/B (N/m)	115,349	0.53
Au = Ay (g)	0.53	0.33

Table 10
Log-normal distribution parameters for fragility curves of URM and CM buildings (wall thickness = 12 cm).

Parameter	Median value	β (sdln)
K_d	1.2*	0.52*
ρ (kg/m^3)	2000*	0.12*
C_d	2*	0.37*
B (m)	7.0	0.21
Fyi (kN)	Table 7	Table 7
Fui (kN)	Table 7	Table 7

* Prieto et al. (2018a).

using the point estimation method for probabilistic moments (Rosenblueth, 1975), as illustrated in Fig. 8. The nonlinear behaviour of masonry was incorporated by idealizing the structural system with the equivalent frame method (wide-column approach) (Gonzales et al., 2020). Using ETABS software, 48 representative buildings were modelled, categorized according to construction typology (URM and CM), architectural configuration (corner, party, and standalone buildings), number of storeys (1 to 4), and average wall thickness (12 cm and 20 cm). This included 24 URM and 24 CM structures. Considering the typical brick arrangements in wall construction, average wall thickness of 12 cm and 20 cm and an inter-storey height of 2.4 m were utilised. In buildings with a wall thickness of 12 cm, an average wall density in the longitudinal direction per floor of 0.049 m^2/m^2 was used, and an average wall density in the orthogonal direction per floor of 0.029 m^2/m^2. For buildings with a wall thickness of 20 cm, an average wall density in the longitudinal direction per floor of 0.082 m^2/m^2 was used, and an average wall density in the orthogonal direction per floor of 0.048 m^2/m^2. The geometric configurations described above are based on prior studies (Acevedo et al., 2017; Adhikari et al., 2023; Yekrangnia, 2023) and complemented by expert judgment. Following Rosenblueth's method, 2^n models were analysed, where *n* is the number of variables considered as random. For the 24 URM structures, uncertainty was incorporated into five variables (c, f'_m, μ, f'_t, σ_v), resulting in 32 simulations per structure, for a total of 768 URM models. Similarly, for the 24 CM structures, uncertainty was modelled in five variables (f'_m, v_m, f_y, $f'c$, σ_v), again leading to 768 models. In total, 1536 models were analysed using the pushover method, a progressive static nonlinear analysis procedure. The distribution of mass movement pressure was assumed uniform across the structures (Luo et al., 2020), with a maximum contact height of 4.8 m. The results of the lateral capacity curve parameters under the rigid base assumption are presented in Tables 7 and 8.

Table 11
Log-normal distribution parameters for fragility curves of URM and CM buildings (wall thickness = 20 cm).

Parameter	Median value	β (sdln)
K_d	1.2	0.52
ρ (kg/m^3)	2000	0.12
C_d	2	0.37
B (m)	7.0	0.21
Fyi (kN)	Table 8	Table 8
Fui (kN)	Table 8	Table 8

Table 12
Fragility curve parameters for URM and CM buildings (1–4 storeys, wall thickness = 12 cm). Intensity: momentum flux.

Structure Type	Median hv^2 (m^3/s^2)				β DS
	Slight	Moderate	Extensive	Complete	sdln
URM 1 Storey	3.55	7.10	7.51	7.89	0.80
URM 2 Storeys	6.69	13.38	14.54	15.69	0.80
URM 3 Storeys	10.88	21.75	22.86	23.95	0.80
URM 4 Storeys	12.66	25.31	26.54	27.75	0.80
CM 1 Storey	9.21	18.42	22.09	25.52	0.70
CM 2 Storeys	16.52	33.05	38.56	43.68	0.70
CM 3 Storeys	27.98	55.95	65.96	75.26	0.70
CM 4 Storeys	32.50	65.00	75.17	84.16	0.70

Table 13
Fragility curve parameters for URM and CM buildings (1–4 storeys, wall thickness = 20 cm). Intensity: momentum flux.

Structure Type	Median hv^2 (m^3/s^2)				β DS
	Slight	Moderate	Extensive	Complete	sdln
URM 1 Storey	5.76	11.53	12.67	13.81	0.84
URM 2 Storeys	10.00	20.02	21.91	23.79	0.80
URM 3 Storeys	14.81	29.63	31.37	33.10	0.80
URM 4 Storeys	19.89	39.79	41.80	43.80	0.80
CM 1 Storey	16.65	33.30	42.40	51.06	0.70
CM 2 Storeys	27.80	55.60	67.15	77.99	0.70
CM 3 Storeys	49.61	99.23	116.94	133.43	0.70
CM 4 Storeys	58.81	117.62	134.76	149.78	0.70

4.4. Masonry structures' fragility curves (fix/rigid foundations)

As discussed in Section 3, fragility curves are used to quantify the vulnerability of buildings. Following standard practice, log-normal functions are adopted to define fragility curves for mass movements, using momentum flux (hv^2) as the hazard intensity parameter—where h and v represent the depth and velocity of the mass movement at a given location, respectively (Prieto et al., 2018b). Each fragility curve is characterized by a median value and a log-normal standard deviation (β). Accordingly, the probability of reaching or exceeding a specific damage state, given the structural response to a defined hazard, is calculated using the following expression:

$$P\left[DS/hv^2\right] = \left[\frac{1}{\beta_{DS}} ln\left(\frac{hv^2}{\overline{\mathrm{hv}^2}_{DS}}\right)\right] \quad (12)$$

where:

hv^2: is the mass movement impact index that represents the intensity of the hazard, Fig. 9.

$\overline{\mathrm{hv}^2}_{DS}$: is the median value of the impact index at which the building reaches the Damage State (DS).

β_{DS}: is the standard deviation of the natural logarithm of the impact index associated with a Damage Stat (DS).

Φ: is the standard normal cumulative distribution function.

Table 14
Fragility curve parameters for URM and CM buildings (1–4 storeys, wall thickness = 12 cm). Intensity: flow depth (height).

Structure Group	Median h (m)				β DS
	Slight	Moderate	Extensive	Complete	sdln
URM 1 Storey	0.40	0.56	0.58	0.59	0.67
URM 2 Storeys	0.54	0.77	0.80	0.83	0.67
URM 3 Storeys	0.69	0.98	1.00	1.03	0.67
URM 4 Storeys	0.75	1.06	1.08	1.11	0.67
CM 1 Storey	0.64	0.91	0.99	1.07	0.54
CM 2 Storeys	0.86	1.21	1.31	1.39	0.54
CM 3 Storeys	1.12	1.58	1.71	1.83	0.54
CM 4 Storeys	1.20	1.70	1.83	1.93	0.54

Table 15
Fragility curve parameters for URM and CM buildings (1–4 storeys, wall thickness = 20 cm). Intensity: flow depth (height).

Structure Group	Median h (m)				β DS
	Slight	Moderate	Extensive	Complete	sdln
URM 1 Storey	0.51	0.72	0.75	0.78	0.70
URM 2 Storeys	0.66	0.94	0.99	1.03	0.67
URM 3 Storeys	0.81	1.15	1.18	1.21	0.67
URM 4 Storeys	0.94	1.33	1.36	1.39	0.67
CM 1 Storey	0.86	1.22	1.37	1.51	0.54
CM 2 Storeys	1.11	1.57	1.73	1.86	0.54
CM 3 Storeys	1.49	2.10	2.28	2.44	0.54
CM 4 Storeys	1.62	2.29	2.45	2.59	0.54

Table 16
Buildings affected by mass movements in South Korea.

Building N°	Flow depth (m)	Flow velocity (m/s)	Momentum flux (m^3/s^2)	Damage State
k-1	0.71	3.2	7.27	Complete
a-4	0.99	3.5	12.13	Complete
a-1	1.33	3.4	15.37	Complete
i-3	1.44	3.5	17.64	Complete
i-2	1.98	3.7	27.11	Complete
b-1	2.7	3.5	33.08	Complete
i-1	3.22	4.2	56.80	Complete
j-1	3.23	6.6	140.70	Complete

Table 17
Summary of fragility curve parameters for complete damage in URM buildings.

Type	Median hv^2 (m^3/s^2)	β DS
	Complete damage	sdln
South Korea field data	24	1.0
URM fragility curve (current research), two stories, 20 cm wall thickness	23.79	0.80
China fragility curve	26	–

The median value corresponds to the point at which the probability of reaching or exceeding the damage state is 50 %, i.e., it defines the threshold value. The standard deviation provides an indication of the dispersion of the fragility curve.

The momentum flux (hv^2) —also referred to as the impact index— is mathematically defined as the product of the mass movement depth and the square of the maximum flow velocity at a given location (Fig. 9). It is recognized as a realistic indicator of the hydrodynamic forces that cause the lateral displacement of buildings and other assets (Jakob et al., 2012). From a physical standpoint, momentum flux reflects the hydrodynamic drag force normalized by the fluid density and the width of the building.

The hydrodynamic force acting on the structure is calculated based on FEMA (2017), as shown in Eq. (13):

Table 19
Summary parameters for fragility curves (momentum flux), complete damage, URM buildings (hv^2 intensity).

Type	Median hv^2 (m^3/s^2)	β DS
	Complete damage	sdln
Salgar, Antioquia, Colombia, data adjustment	7.0	0.86
URM fragility curve (current research), single storey, 12 cm wall thickness	7.89	0.80

$$F_a = \frac{K_d}{2} C_d . \rho . B \left(hv^2\right) \tag{13}$$

The impact coefficient (K_d) adjusts the hydrodynamic force to account for the size of the material transported by the mass movement, which may intensify the force and increase the potential for damage. The drag coefficient (C_d) is included in the model to account for the resistance created by the interaction between the moving mass and the structure. The parameter ρ represents the density of the mass movement material, which varies depending on the type of phenomenon. The building width (B) is measured perpendicular to the direction of the flow. Each random variable used in the formulation is represented by a lognormal distribution function.

The structural capacity thresholds in response to mass movements are defined based on varying damage states, as illustrated in Fig. 10 and described below:

Slight Damage State. Occurs when the mass movement hazard equals half the building's yield strength at the base (Kean et al., 2019).

$$F_{r\ elastic} = \frac{F_y}{2} \tag{14}$$

Moderate Damage State. Defined as the point at which the hazard equals the building's basal yield strength.

$$F_{r\ yield} = F_y \tag{15}$$

Extensive Damage State. Occurs when the hazard reaches the average of the building's yield and ultimate strength.

$$F_{r\ extensive} = \frac{F_y + F_u}{2} \tag{16}$$

Complete Damage State. Reached when the hazard exceeds the building's ultimate strength.

$$F_{r\ complete} = F_u \tag{17}$$

The acting mass movement force (Eq. 13) can be matched with the building's lateral capacity expressions (Eqs. 14, 15, 16, and 17) to solve for the momentum flux threshold, hv^2, associated with each damage state, as shown in Eq. (18):

$$hv^2 = \frac{2F_r}{K_d . C_d . \rho . B} \tag{18}$$

By incorporating the uncertainty parameters of each variable, it

Table 18
Buildings affected by mass movements in Salgar, Antioquia, Colombia (DAPARD, 2015).

Building N°	Latitude	Longitude	Flow depth (m)	Flow velocity (m/s)	Momentum flux (m^3/s^2)	Damage State
7	5.958577	−76.006682	0.45	2.52	2.84	Complete
5	5.95879	−76.006511	0.44	3.06	4.14	Complete
4	5.958832	−76.006497	0.57	2.95	4.98	Complete
6	5.958731	−76.006571	0.64	2.87	5.26	Complete
3	5.958879	−76.006485	0.7	3.44	8.25	Complete
2	5.95896	−76.006332	1.11	3.57	14.1	Complete
1	5.95901	−76.006252	1.19	3.76	16.88	Complete

Note. All affected buildings were single-storey URM structures with an average wall thickness of 12 cm and lightweight asbestos-cement roofing.

Table 20
Summary parameters for fragility curves (flow height), complete damage, URM buildings (h intensity).

Type	Median h (m)	β DS
	Complete damage	sdln
Salgar, Antioquia, Colombia data adjustment	0.70	0.55
URM fragility curve (current model), single storey, 12 cm wall thickness	0.59	0.67

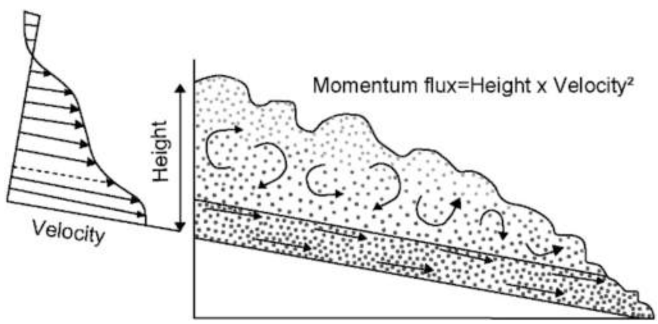

Fig. 9. Impact index or momentum flux.

becomes possible to estimate the median momentum flux, $\overline{hv^2}_{DS}$, and its standard deviation, β_{DS}, as illustrated in Fig. 11.

4.5. Application of the proposed method

Previous research estimated fragility curves for the complete damage state of URM buildings under mass movements (Prieto et al., 2018b). That study obtained a median threshold value for momentum flux of 23.32 m^3/s^2 and a log-normal standard deviation of 0.899. The analysis was conducted in Medellín, Colombia, on 40 buildings ranging from 1 to 4 storeys, all with an average wall thickness of 20 cm. The researchers employed typical earthquake-based assumptions to estimate buildings' lateral capacity and uncertainty, drawing from sources such as Acevedo et al. (2017). The resisting force (Fr) for the complete damage state was calculated using seismic parameters (Au, Ay), gravitational loads (W), building width (B), modal seismic parameters (α), and over-resistance factors (λ), in accordance with FEMA (2012), as summarized in Table 9.

The current methodology improves upon that proposal by incorporating the structural behaviour of URM and CM buildings specifically under mass movement loads. Parameters used for wall thicknesses of 12 cm and 20 cm are presented in Tables 10 and 11.

The parameters for fragility curves —median values and log-standard deviations— are summarized in Tables 12 and 13. Graphical representations are included in Appendix A.

Additionally, fragility curves were generated using the mass movement height at impact as an alternative intensity measure. The acting hydrostatic force was calculated based on Armanini (2008).

$$Fa = \frac{C_S}{2}\rho g h^2 B \tag{19}$$

Here, gravity is 9.81 m/s^2. C_S is a dimensionless coefficient that accounts for the overpressure effect due to the dynamic behaviour of the flow (Hu et al., 2011; Huebl et al., 2017; Vagnon and Segalini, 2016); ρ is the density of the material; h is the depth (or height) of the mass movement; and B is the width of the structure. Due to the availability of only extreme data, the coefficient C_S is represented by a continuous uniform probability distribution function. The distributions for density and building width are as previously defined. By matching the acting lateral force expression (Eq. 19) with the corresponding capacity levels (Eqs. 14, 15, 16, and 17), threshold heights and their associated uncertainties were derived and are presented in Tables 14 and 15. Graphical representations are included in Appendix B.

5. Validation

The results of the proposed model were compared with field data obtained from case studies in South Korea and Colombia. One of the main challenges in validating fragility models for mass movements lies in the limited availability of published data that report both hazard intensity measures (e.g., flow depth and velocity) and detailed structural classification of the affected buildings, including observed damage states. A comprehensive database of 68 mass movement events compiled by Jakob et al. (2012) includes relevant hazard parameters —flow depth, velocity, and momentum flux (minimum, average, and maximum)— but unfortunately omits structural typologies and damage classification schemes (e.g., HAZUS system). As a result, these data cannot be directly used to test fragility models based on structural performance. In Southwest China, 61 buildings were affected by the August 20, 2019 mass movement event in Cutou Gorge, Wenchuan, of which 19 were unreinforced masonry (URM) structures ranging from one to two storeys in height. According to Chen et al. (2021), this event verified a mean momentum flux threshold of 26 m^3/s^2 for a complete damage state. While detailed information on each individual structure

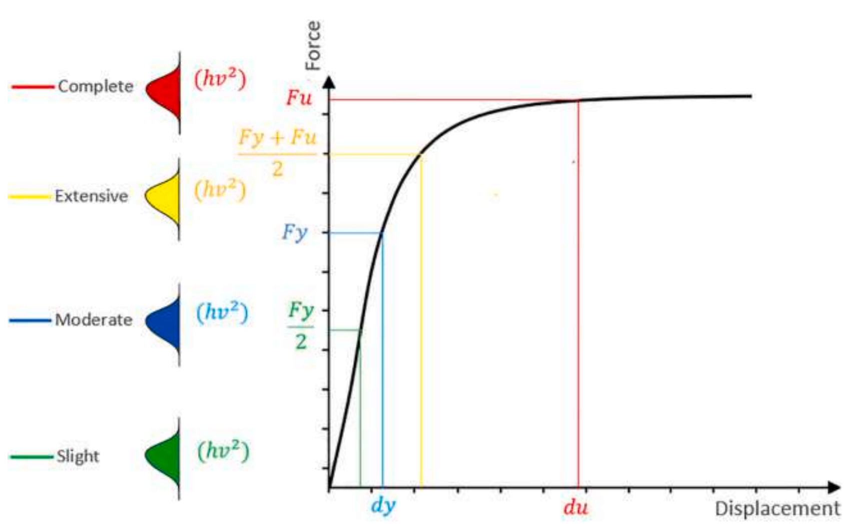

Fig. 10. Structural capacity curve used in the probabilistic analysis.

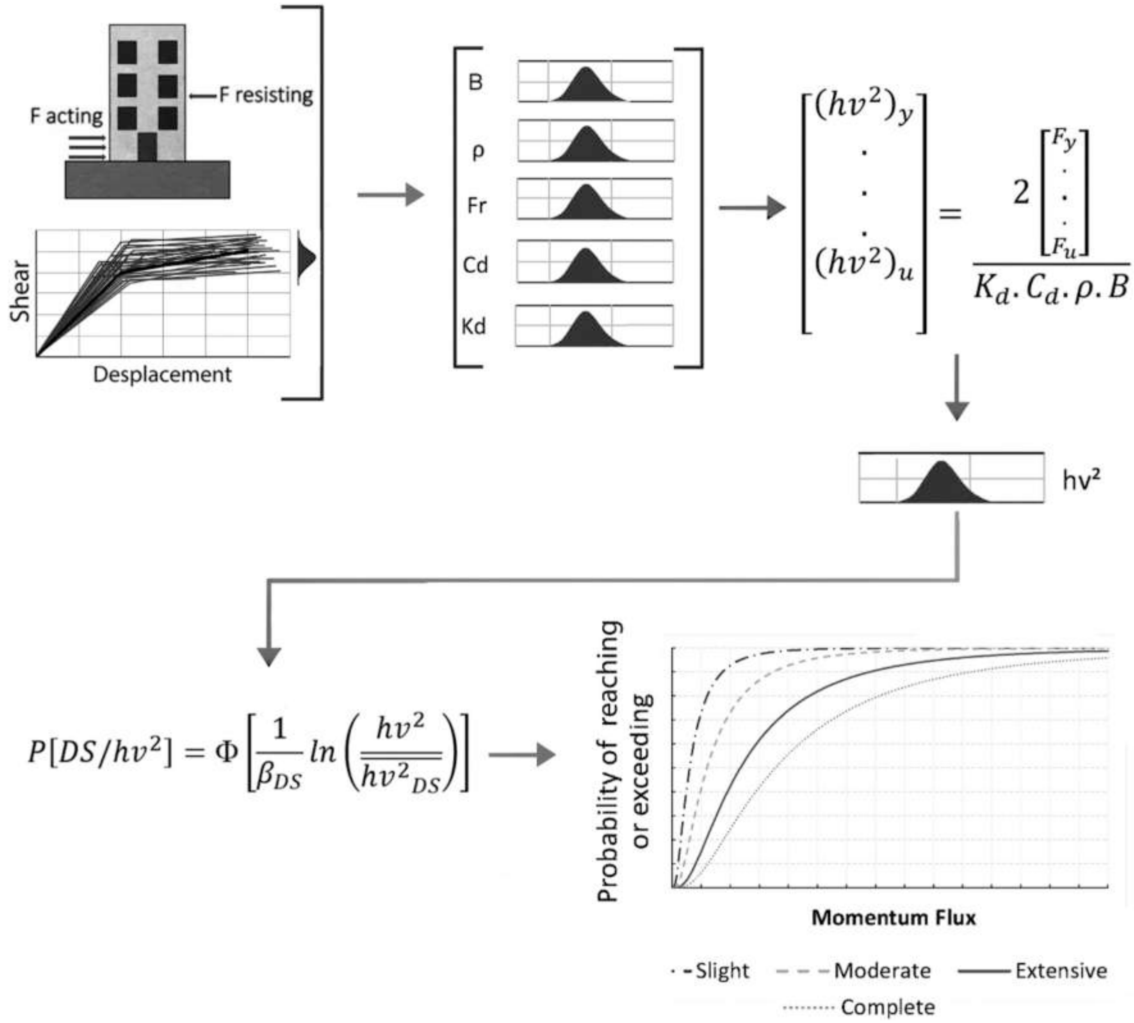

Fig. 11. Methodology for determining building fragility curves corresponding to different damage states.

was not available, visual analysis of images suggests an average wall thickness of approximately 20 cm. For the purposes of this study, we were able to compile sufficient and relevant data from two additional sources: The South Korean dataset published by Kang and Kim (2016) and a mass movement event in Colombia that occurred in 2015. These two cases are described in more detail in the following sections.

5.1. Data from South Korea

A dataset that includes both hazard parameters and specific structural data is provided by Kang and Kim (2016). These authors collected and analysed detailed information from 25 buildings affected by 11 mass movement events in South Korea. For each site, they reported flow depths, velocities, and impact pressures, and also classified the building types and damage states according to the HAZUS system. Using the reported depth and velocity data, we calculated the momentum flux for each building. Results for the URML buildings —the most abundant category in the dataset— are presented in Table 16. This group includes eight unreinforced masonry (URM) buildings, between one and two storeys, all of which experienced complete damage.

An approximate cumulative distribution function was generated using rank probability (i.e., sorting the momentum flux values from lowest to highest and dividing each rank by the total number of observations to obtain a probability). This empirical curve is plotted as dots in Fig. 12. A log-normal fragility curve was fitted to the field data, yielding a median momentum flux of 24 m^3/s^2 and a log-normal standard deviation (β) of 1.0.

Fig. 12 and Table 17 highlight the strong agreement between the empirical fragility curve based on South Korean field data and the model-derived fragility curve from the current study for URM buildings with 20 cm wall thickness and two storeys. The median values are remarkably similar —ranging from 23 to 26 m^3/s^2— and represent the thresholds at which complete damage is expected due to mass movement impact.

While the S-shaped fragility curves proposed by Chen et al. (2021) differ in form from the fitted curve based on South Korean data and the function proposed here, the complete damage threshold is consistent, as shown in Table 17.

5.2. Intensity parameters and physical damage in buildings due to the mass movement occurred in Salgar, Antioquia, Colombia

In the early morning of May 18, 2015, intense rainfall occurred in the upper basin of the Liboriana Creek, located in the municipality of Salgar, department of Antioquia, Colombia. These rains triggered a series of debris flows that converged through multiple channels and rapidly descended toward the lower basin in the form of a torrential flood. Along its path, the mass movement destroyed approximately 90 houses, claimed the lives of 94 individuals, left 11 missing, and impacted an estimated 1397 people.

To estimate the hazard intensity parameters (flow depth h and velocity v) required for the validation of the proposed methodology, a

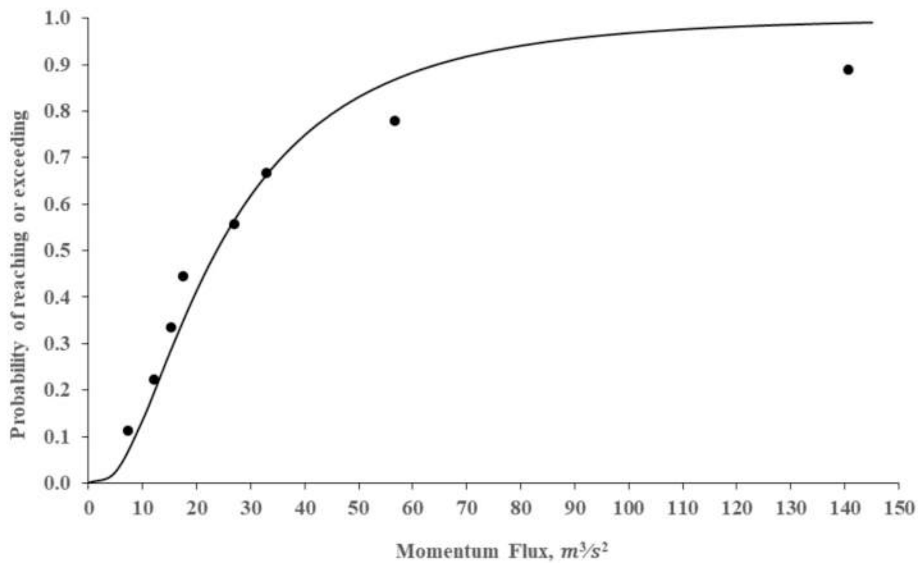

Fig. 12. Fragility curves for complete damage in URM buildings from two sources: South Korea field data (dots) and the current research model (solid line) for two-storey buildings with an average wall thickness of 20 cm.

hydraulic model of the Liboriana stream was developed using HEC-RAS v6.5. The simulation was based on updated 2023 topography and represented a 300-year return period flow scenario, with a 40 % increase in discharge to account for sediment contribution. The results of the 2D model provided the spatial distribution of flow depth (Fig. 13) and velocity (Fig. 14), which were then used to calculate momentum flux (hv^2) at the location of the affected buildings.

It is important to note that the model was run using post-event topography. Photographic evidence suggests that, prior to the 2015 event, the channel was shallower, which could imply that the modelled

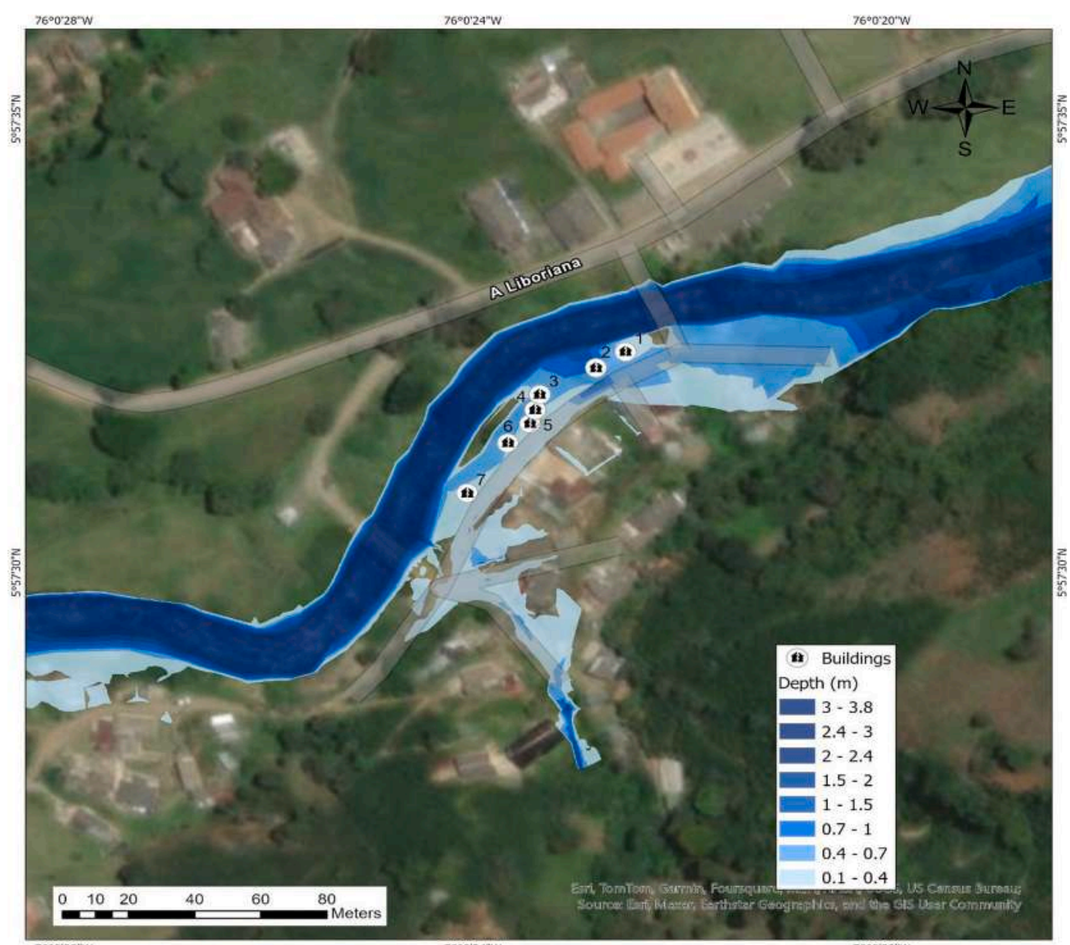

Fig. 13. Flow depth for the 300-year return period debris flow (free water surface).

momentum flux values are conservative compared to the original conditions.

The description of the building damage was taken from the report prepared by the Administrative Department of Disaster Prevention, Response, and Recovery System of Antioquia (DAPARD, 2015), based on several field visits conducted between March 18 and 22, 2015. In this report, the destroyed or damaged houses located in different sectors of the municipality along the Liboriana Creek were identified and georeferenced using geographic coordinates. Additionally, photographic evidence included in the report documented the condition of the affected structures (Fig. 15). Based on this information, it was possible to geolocate the impacted houses and assign to each of them the corresponding maximum momentum flux values, as presented in Table 18.

Fig. 15 shows one of the areas where the destroyed houses were located, of which only the foundation slabs remain.

To validate the proposed fragility curves, a rank-based cumulative distribution of momentum flux values was generated. As shown in Fig. 16, there is a strong agreement between field data and the model-derived fragility curve for single-storey URM buildings with 12 cm walls. This correspondence is further supported by the summary presented in Tables 19 and 20.

6. Discussion

Assessing physical vulnerability due to mass movements is essential for reducing risk and enhancing regional resilience. Despite advances in understanding the interaction between mass movement hazards and structural fragility, vulnerability assessment remains a weak component in quantitative risk analyses (Huang et al., 2023a; Luo et al., 2023). This gap is even more pronounced for URM and CM buildings, which comprise a significant portion of residential and informal constructions globally. Although no HAZUS module currently exists for mass movements, the methodology developed for tsunamis serves as a benchmark for calculating structural fragility due to these hazards, as demonstrated by Kean et al. (2019) and Prieto et al. (2018a). However, it is important to note that those studies relied on seismic design parameters to estimate structural capacity (Luo et al., 2023). This paper introduces a model for the structural behaviour of URM and CM buildings subjected to lateral loads from mass movements, without relying on seismic parameters. The methodology is particularly suited for less developed regions where laboratory and field data are scarce, sophisticated equipment is unavailable, and time constraints are pressing. The three-dimensional mechanical behaviour of URM and CM buildings is studied, emphasizing the role of the global structural performance of the buildings in the shear resistance offered by the walls to in-plane lateral loads. This concept is based on the great rigidity and resistance that these walls offer

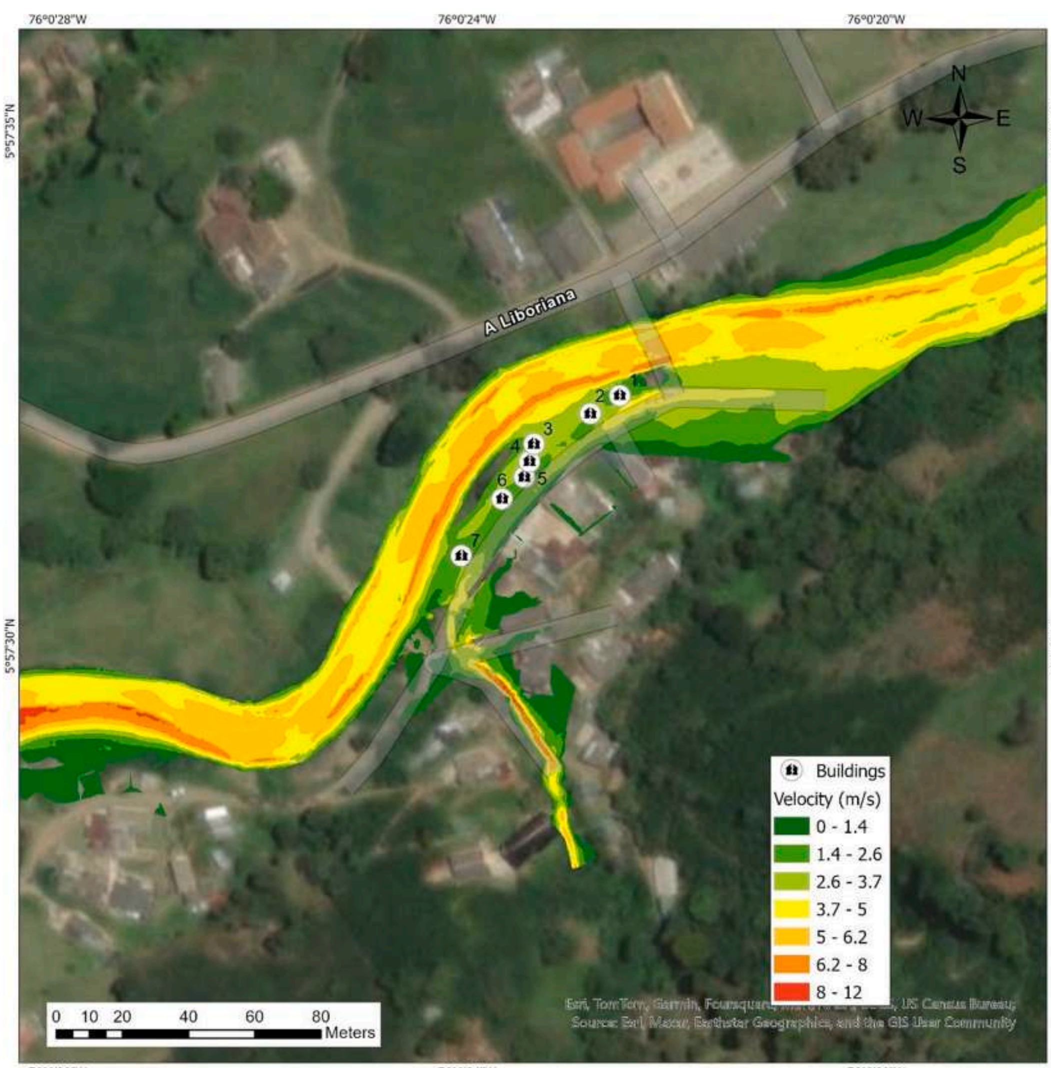

Fig. 14. Flow velocity for the 300-year return period debris flow (free water surface).

Fig. 15. View of Margarita Village downtown affected by the torrential floods.

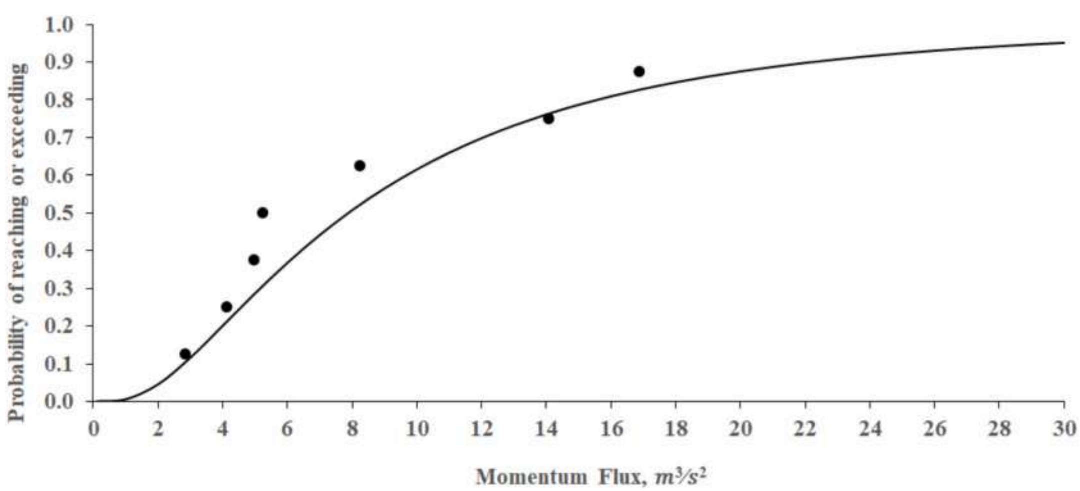

Fig. 16. Fragility curves for complete damage in URM buildings based on momentum flux (hv^2): Salgar field data (dots) vs. current research model (solid line).

in-plane, being responsible for providing lateral stability to the building against mass movements. Without knowing the direction of attack of the flow against buildings, three-dimensional models (assuming a fixed/rigid base) were analysed using the nonlinear pushover method. Each structure was loaded independently in its two main orthogonal directions, choosing the most critical response in terms of shear capacity. The macro-modelling approach using equivalent frames (Section 4.1) proved to be an effective tool for this study, allowing the capture of the global behaviour of masonry structures and the performance of nonlinear ('pushover') analysis with a manageable computational cost, in line with previous findings on its efficiency (Ahmed et al., 2019).

The Rosenblueth simulation method offers an effective and efficient probabilistic tool for determining the lateral structural capacity of three-dimensional models, specifically in terms of shear strength and associated uncertainties. In comparison to the use of micromodels or detailed finite element models that account for dynamic interactions with impact loads —along with Monte Carlo simulations— the differences in computational cost, required resources, and processing time are substantial. Moreover, its application to complex structures remains limited (Asteris et al., 2014; Thinley and Hao, 2017). To derive fragility curves or damage thresholds by equating structural capacity with hazard intensity from mass movements, it is feasible to use an analytical function based on momentum flux, flow height, or another relevant intensity measure. Once such a function is defined, Monte Carlo simulation can be employed to estimate probabilistic responses. However, in this study, the cumulative distribution function adopted is the log-normal distribution, which is widely accepted in engineering due to its strong empirical fit. This choice allows the analysis to be conducted efficiently, even within a spreadsheet environment.

Model results highlight a good agreement with damage field data. In the case of 2-storey thick walls (~20 cm) URM buildings, complete damage threshold values range between 23 and 26 m^3/s^2 for South Korea, Wenchuan in China, and this research (Fig. 12; Table 17). On the other hand, data from Salgar, Antioquia, Colombia, indicate, for 12 cm wall thickness URM buildings, a slightly lower, but not significantly different, threshold momentum flux field value of 7 m^3/s^2 as compared to 7.89 m^3/s^2 for the model (Fig. 16; Table 19). Using the mass movement height, h, as an intensity parameter, no significant difference is noted between field data and model results, i.e., 0.70 m against 0.59 m respectively (Fig. 17; Table 20). The main differences between field data and model results can be attributed, for example, to the fact that before the 2015 event, the Liboriana Creek channel had different topographic sections than it has today, which may affect the hydraulic modelled values compared to those of the original event. Another parameter that deserves some comment is the standard deviation. Previous research indicated log standard deviations in the order of 0.90 for momentum flux intensity thresholds in URM buildings (Prieto et al., 2018a), while lower values, e.g., 0.80, were obtained in this research (Tables 12 and 13). This reduction in epistemic uncertainty is attributed to the use of the three-dimensional structural modelling approach adopted in this study.

An important consideration when evaluating the agreement between the proposed model and the field data from South Korea (Kang and Kim, 2016) and Salgar, Colombia (DAPARD, 2015) is the possible influence of differences in building regulations, local construction practices, and specific material properties between the two geographical regions. It is reasonable to assume that these differences could induce variations in the actual resistance of the buildings to the impact of mass movements, which raises questions about the direct comparability of these data sets with a generalized model such as ours. Nevertheless, it is essential to contextualize this comparison within the scope and specific objectives of this study. The model and fragility functions developed here seek to represent, as a priority, the vulnerability of unreinforced masonry (URM) and confined masonry (CM) buildings characteristic of informal construction or buildings constructed to low standards or not strictly regulated. This construction typology is unfortunately very common in numerous highly dangerous areas around the world, including Colombian in the Andean Region and potentially representative of the URML structures reported in the South Korean data set used for validation. For this class of buildings, it is postulated that the fundamental response characteristics (low ductility, failure modes dominated by shear in walls) and the inherent variability of materials and workmanship may have a greater influence than the specific differences between national high-level design codes, whose strict application in this construction segment may be limited. The mechanical parameters and their uncertainties (Tables 2 and 3) were selected to reflect this generalized condition. In addition, the probabilistic nature of the methodology, through the use of the Rosenblueth method and the characterization of fragility with log-normal curves that include a standard deviation (β) (Tables 12–15), allows for the incorporation and reflection of a part of the expected variability in structural performance, which can come from both parameter uncertainty and constructive differences between different buildings or regions. The validation also focused on comparing the results for building typologies that are as similar as possible (mainly 1–2-storey URM) between the field data and the model. Considering these aspects, the reasonable agreement observed in the validation, particularly in the thresholds for the state of complete damage (Figs. 12 and 16; Tables 17 and 19), is encouraging. It suggests that, despite the undoubted contextual differences, the proposed model manages to capture fundamental aspects and general trends in the vulnerability of this kind of low-standard masonry building in different geographical environments. It therefore provides a useful and generalizable tool for preliminary assessments or in regions where there is no detailed local data. However, we recognize as a limitation that perfect transferability cannot be assumed; ideally, fragility functions should be calibrated or adapted locally whenever the availability of region-specific data and resources allow for a more accurate vulnerability and risk assessment.

Confining the walls (CM structures) and/or increasing their thickness improves the structural performance of buildings, as confirmed by the damage state thresholds. For example, for one-storey buildings, complete damage thresholds increase from 7.89 m^3/s^2 in URM constructions to 25.52 m^3/s^2 in CM buildings (Table 12). The complete damage thresholds for two-storey URM buildings with wall thicknesses of 12 cm and 20 cm are 15.69 m^3/s^2 and 23.79 m^3/s^2, respectively (Tables 12 and 13).

The existence or not of a rigid diaphragm (usually a reinforced concrete mezzanine slab) attached to the walls and the gravity loads present in the buildings substantially influence the behaviour of the structures against mass movements. For example, in single-storey buildings with a light roof, the momentum flux damage thresholds are

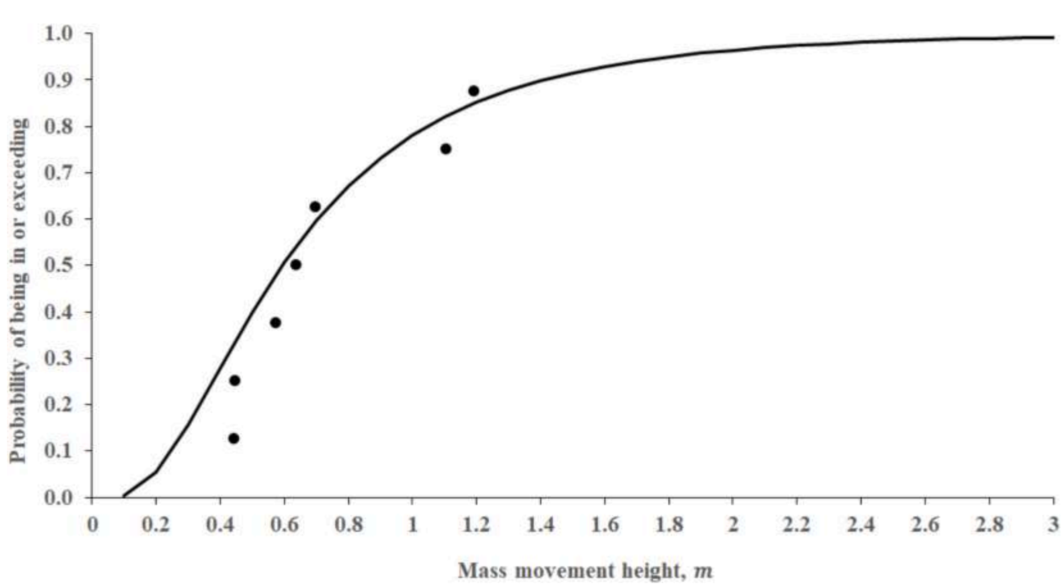

Fig. 17. Fragility curves for complete damage in URM buildings based on flow depth (h): Salgar field data (dots) vs. current research model (solid line).

about half the magnitude present for two-storey buildings, i.e., from 7.89 m^3/s^2 to 15.69 m^3/s^2 in URM buildings (Table 12).

Masonry structures, particularly URM buildings, respond to events like mass movements based on the stiffness and strength of their walls; the possibility of these buildings performing in the inelastic range is limited, as evidenced by the minimal variation in moderate, extensive, and complete damage state thresholds for each building (Tables 12–15) and graphically illustrated in Appendices A and B.

Given the damage thresholds in this study for URM and CM buildings, it is advisable to review the damage thresholds used in the Methodological Guide for Torrential Flood Hazard Zoning (Ramos Cañón et al., 2021). This document uses qualitative information based on Jakob et al. (2012), to derive damage thresholds in terms of momentum flux. The authors determine a damage threshold of 1 m^3/s^2 for light damage, between 1 m^3/s^2 and 50 m^3/s^2 for moderate/severe damage, and greater than or equal to 50 m^3/s^2 for complete damage. For example, the complete damage thresholds for one-storey and two-storey buildings of the URM type (Table 12), equal to 7.89 m^3/s^2 and 15.69 m^3/s^2, differ significantly from the thresholds found in the guide.

It is worth noting that some facade walls might be subjected to out-of-plane loads during a mass movement. These walls will respond with low bending, leading to local failure modes. Although the general methodology presented allows for the analysis of this case, this study focused on the analysis of the structure's global failure.

Hydrodynamic and hydrostatic models were used to quantify hazard intensity and find the damage thresholds and fragility curves. The hydrodynamic model, in terms of momentum flux (hv^2), is essential when the kinetic component is significant; the hydrostatic model, in terms of impact height of the flow (h), can be relevant when the flow loses velocity and turbulence and the gravitational potential component increases. Lastly, while the general methodology considers structural damage from permanent ground deformation, this aspect was not developed in the present study. Addressing it should be a priority for future research.

7. Conclusions

This study reviewed the literature on structural vulnerability to mass movements in urban and rural areas, highlighting a recognized need to quantify vulnerability through the use of fragility curves. It is estimated that in underdeveloped countries, at least 70 % of the building stock consists of masonry structures (URM and CM). Accordingly, the development of a clear and computationally efficient methodology to estimate damage state thresholds for these building types is essential for effective risk reduction.

The global structural vulnerability of buildings to mass movements was assessed by examining the shear failure mechanisms of URM and CM typologies. The study presents an efficient procedure for calculating damage state thresholds and their associated uncertainties—offering a practical balance between analytical rigor, computational cost, and ease of implementation.

Thresholds are provided for four levels of structural damage —slight, moderate, extensive, and complete— for URM and CM buildings ranging from one to four storeys, with two representative wall thicknesses (12 and 20 cm). Fragility curves are presented as functions of both momentum flux and flow height.

Although empirical field data linking hazard intensity to structural damage remain limited, the proposed model shows good agreement with available datasets, including a mass movement database from South Korea and field data from an event in Colombia. These validations support the robustness of the model.

The damage thresholds proposed, along with their quantified uncertainty, are intended to represent informally constructed masonry buildings—common in underdeveloped regions where construction standards are often inadequate. Mechanical properties of masonry were compiled from a range of sources, including empirical studies and expert knowledge. While the results may not be directly transferable to all contexts, the methodology itself is flexible and easily adaptable.

Overall, the proposed methodology offers a meaningful contribution to the understanding of physical vulnerability in clay brick masonry buildings exposed to mass movement hazards. It is computationally accessible, straightforward to implement, and adaptable to multi-hazard risk frameworks—including those addressing earthquakes, permanent ground failure, and Natech events. As such, it represents a valuable tool for reducing disaster risks, particularly in data-scarce and resource-limited settings that are affected by climate variability.

Nomenclature

$\underline{(hv^2_{DS})}$	Median value of the impact index at which the building reaches a damage state threshold
A	Effective or net cross-sectional shear area of masonry
Au	The ultimate strength of the building in terms of seismic acceleration
Ay	The yield strength of the building in terms of seismic acceleration
B	Plan dimension of the building. The direction of mass movements is perpendicular to this dimension
c	Cohesion
cd	Drag coefficient
db	The diameter of the longitudinal reinforcement
E(Y)	Expected value of the function
Em	Masonry elasticity modulus
Fa	Hydrodynamic or hydrostatic acting force
f'c	Specified compressive strength of the concrete
f'cb	Specified compressive strength of the bricks
f'm	Specified compressive strength of the masonry
Fr	The building-resistant force for different damage state thresholds
f'tb	Specified tensile strength of the bricks
Fu	The buildings' ultimate strength
fy	Yield strength of the longitudinal reinforcement
Fy	The basal yield strength of the building
Gm	Modulus of stiffness in shear of the masonry
h	Height brick, debris flow depth
H	The effective height of the wall
hv^2	Momentum flux or impact index
Ic	Moment of inertia of the confining columns of the wall
Im	Wall section inertia
Is	Moment of inertia of the longitudinal steel of columns of the wall
Kd	Impact coefficient
Ke	Stiffness in the elastic range
L	Wall length
l	Length brick
n	Number of longitudinal bars in the wall, number of variables to correlate in the Rosenbluth method
Pij..n	Weighting factors
qult	The ultimate strength of the out-of-plane walls
S(Y)	The standard deviation of the function
t	The effective thickness of the wall
v	Debris flow frontal velocity
V_1	Shear strength due to friction-shear failure mode. URM walls
V_2	Shear strength due to diagonal tension failure mode. URM walls
V_3	Shear strength due to compression failure mode. URM walls
Vcr	Cracking shear strength. CM walls
vm	Diagonal compressive strength of masonry
Vmax	Maximum shear strength. CM walls
Vult	Ultimate shear strength. CM walls
W	Gravitational loads present in the structure

α Modal parameter
β Factor that depends on the support conditions at the ends of the wall, Standard deviation of the natural logarithm of a variable
β_{DS} Standard deviation of the natural logarithm of the impact index associated with a damage state
γ Shape factor
η Efficiency factor
λ Over-resistance factor, coefficients for fixed H/t ratios
μ Masonry friction coefficient
ρ Debris flow density
ρij..n Correlation coefficients
σv Vertical compressive load on the wall
Φ The standard normal cumulative distribution function

Abbreviations

CM Confined clay brick masonry
URM Unconfined, unreinforced clay brick masonry
sd The standard deviation of a variable
$P_{SDI}(DS \geq ds)$ Probability of reaching or exceeding a state of damage in the building, given that structural deformations occur in it due to the impact (Rigid base assumption)
$P_{GF}(DS \geq ds)$ Probability of reaching or exceeding a state of damage in the building foundations, given that there are permanent ground deformations
Pcomb(DS ≥ ds) The combined probability of reaching or exceeding a state of damage, given that the structure shows deformations due to debris flow impact or loss of support due to permanent deformations of the ground
Pcomb(DS = ds) The combined probability of being in a state of damage, given that the structure presents deformations due to debris flow impact or loss of support due to permanent deformations of the ground.
Pcomb(DS ≥ C) The combined probability of reaching or exceeding complete damage state, given that the structure shows deformations due to debris flow impact or loss of support due to permanent deformations of the ground.

CRediT authorship contribution statement

Alfer L. Silva-Ceron: Writing – review & editing, Writing – original draft, Visualization, Validation, Supervision, Software, Resources, Project administration, Methodology, Investigation, Funding acquisition, Formal analysis, Data curation, Conceptualization. **Jorge A. Prieto:** Writing – review & editing, Writing – original draft, Visualization, Validation, Supervision, Software, Resources, Project administration, Methodology, Investigation, Funding acquisition, Formal analysis, Data curation, Conceptualization. **Marco F. Gamboa:** Writing – review & editing, Writing – original draft, Visualization, Validation, Supervision, Software, Resources, Project administration, Methodology, Investigation, Funding acquisition, Formal analysis, Data curation, Conceptualization.

Informed consent statement

Not applicable.

Institutional review board statement

Not applicable.

Funding

This research received external funding from the Ministry of Science, Technology, and Innovation (COLCIENCIAS) as part of the Bicentennial Scholarship programme.

Declaration of competing interest

The authors declare no conflict of interest.

Acknowledgements

The authors gratefully acknowledge the support provided by Dr. Carlos Estuardo Ventura (Professor of Civil Engineering and Director of EERF The University of British Columbia); Dr. Juan Diego Jaramillo Fernández (Retired Emeritus Professor School of Applied Sciences and Engineering EAFIT University, Colombia); Dr. Juan Camilo Molina Villegas (Professor School of Applied Sciences and Engineering EAFIT University, Colombia); MSc. Julio Cesar Diago Franco (Professor of Civil Engineering at the University of Cauca, Colombia); GIS Engineer Emilio Jose Hoyos Valencia (Nacional University, Colombia) and MSc. Ana Carolina Rivera Aguirre (EAFIT University, Colombia).

Appendix A. Appendix

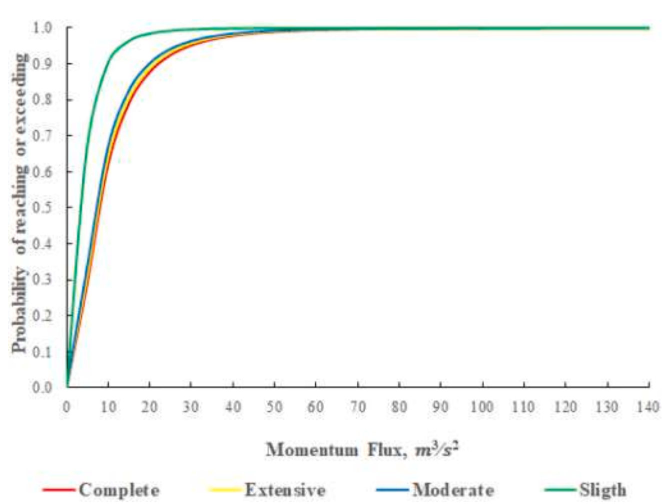

Fig. A1. Fragility curve for 1-storey URM buildings with an average wall thickness of 12 cm. Intensity parameter: momentum flux.

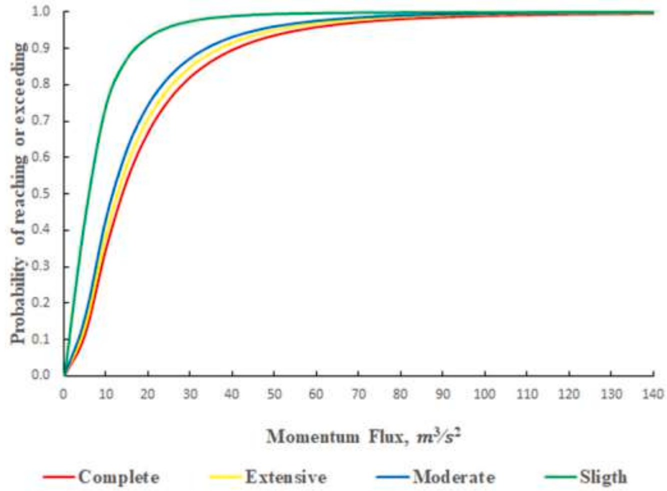

Fig. A2. Fragility curve for 1-storey URM buildings with an average wall thickness of 20 cm. Intensity parameter: momentum flux.

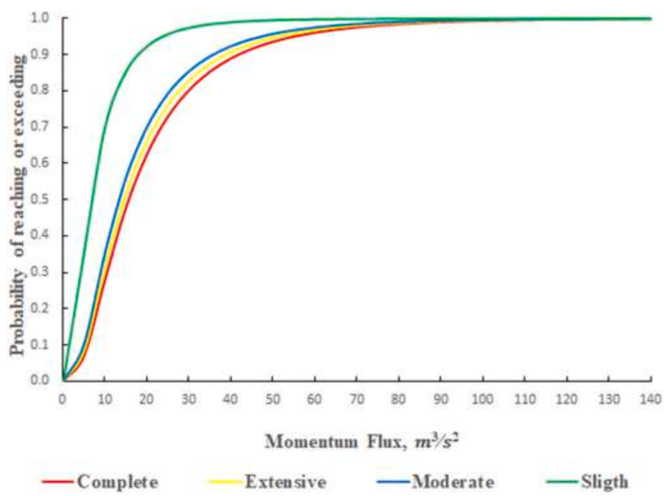

Fig. A3. Fragility curve for 2-storey URM buildings with an average wall thickness of 12 cm. Intensity parameter: momentum flux.

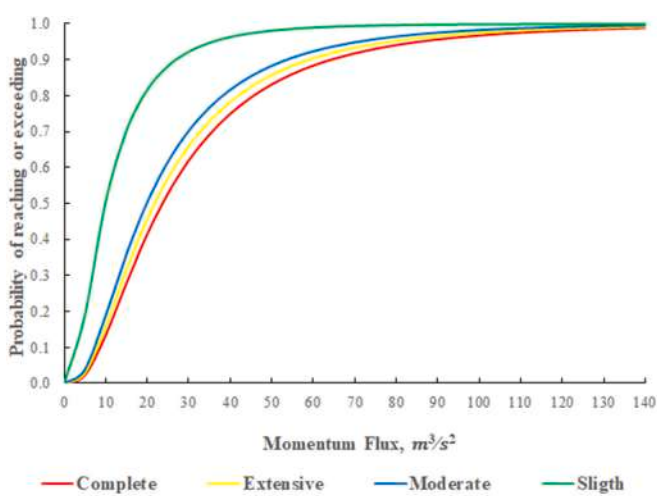

Fig. A4. Fragility curve for 2-storey URM buildings with an average wall thickness of 20 cm. Intensity parameter: momentum flux.

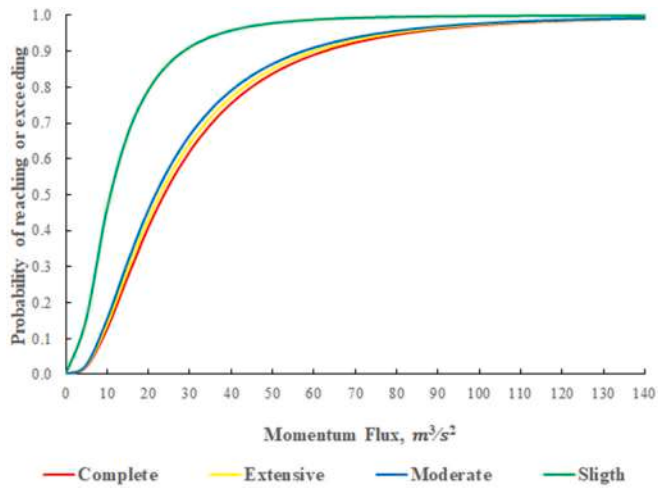

Fig. A5. Fragility curve for 3-storey URM buildings with an average wall thickness of 12 cm. Intensity parameter: momentum flux.

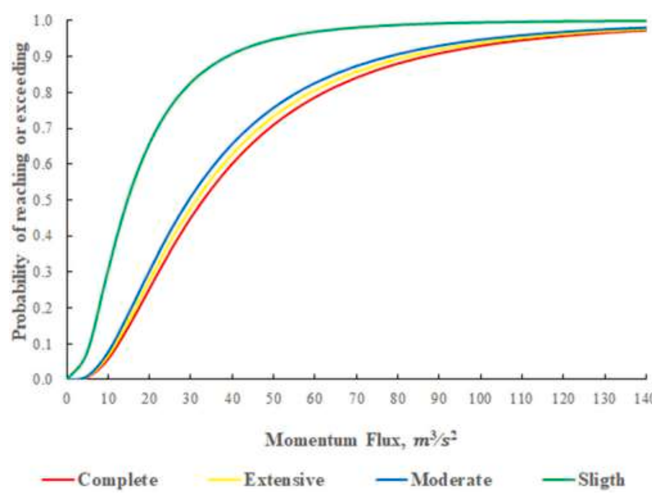

Fig. A6. Fragility curve for 3-storey URM buildings with an average wall thickness of 20 cm. Intensity parameter: momentum flux.

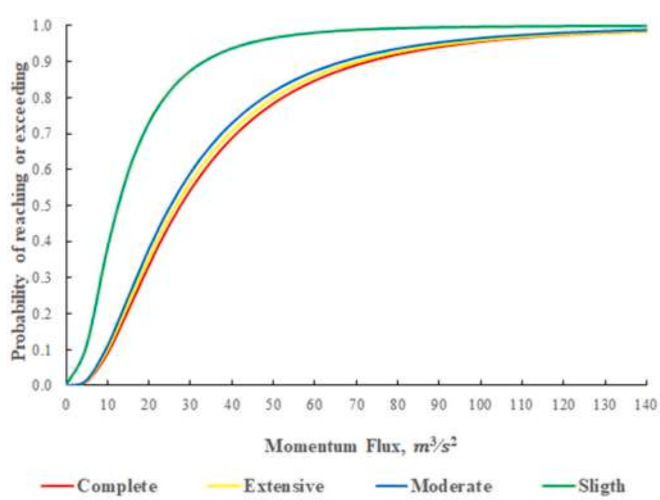

Fig. A7. Fragility curve for 4-storey URM buildings with an average wall thickness of 12 cm. Intensity parameter: momentum flux.

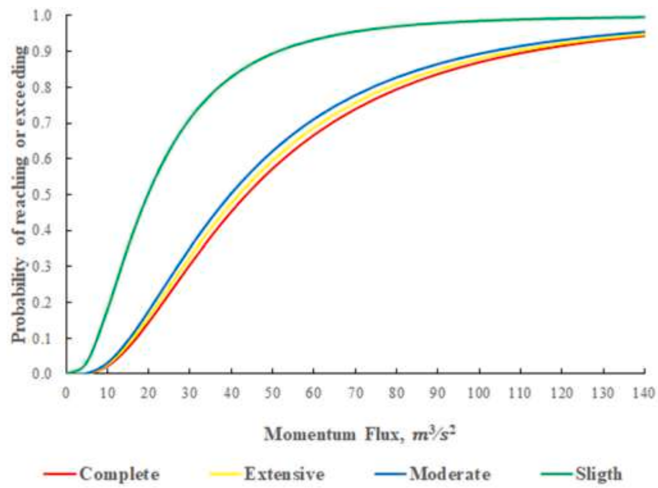

Fig. A8. Fragility curve for 4-storey URM buildings with an average wall thickness of 20 cm. Intensity parameter: momentum flux.

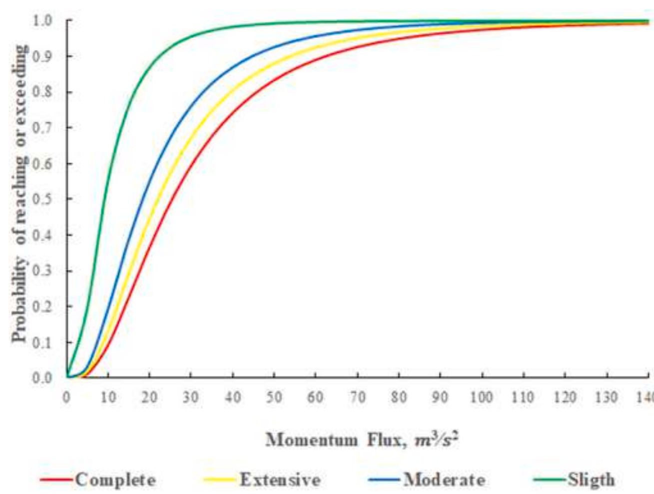

Fig. A9. Fragility curve for 1-storey CM buildings with an average wall thickness of 12 cm. Intensity parameter: momentum flux.

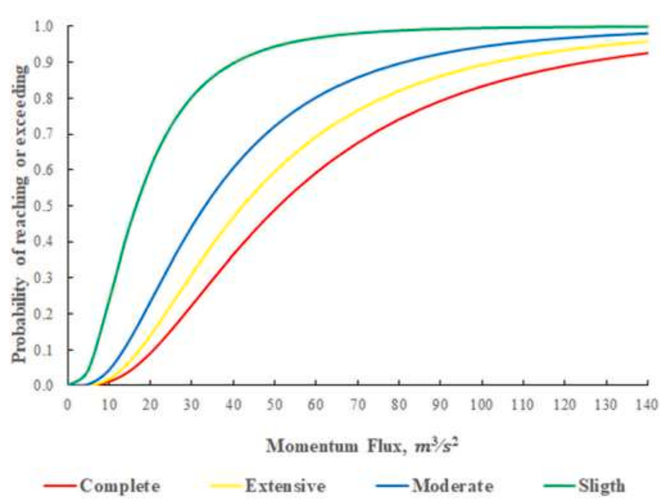

Fig. A10. Fragility curve for 1-storey CM buildings with an average wall thickness of 20 cm. Intensity parameter: momentum flux.

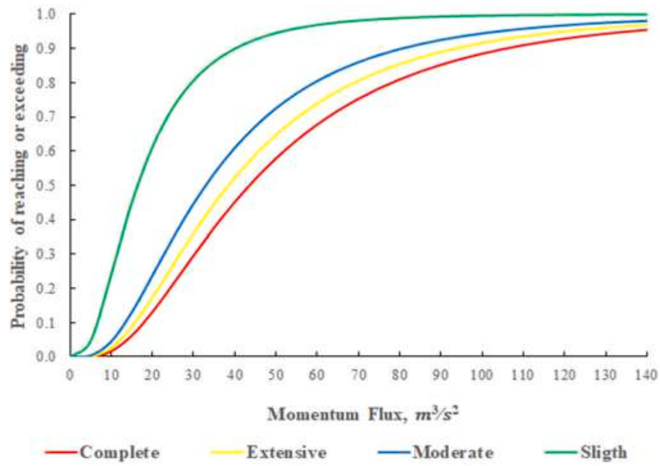

Fig. A11. Fragility curve for 2-storey CM buildings with an average wall thickness of 12 cm. Intensity parameter: momentum flux.

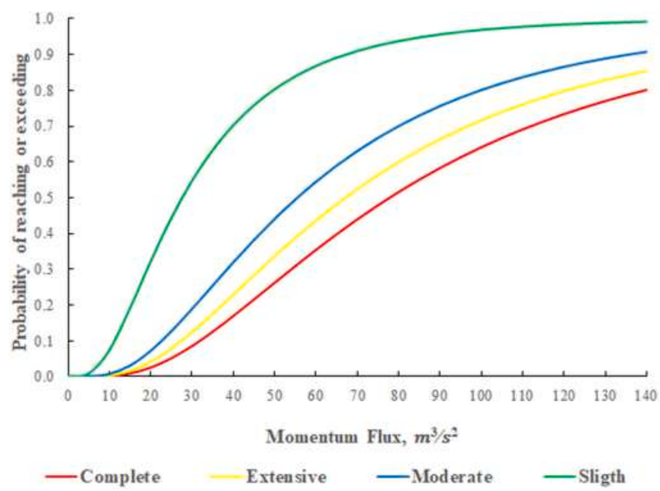

Fig. A12. Fragility curve for 2-storey CM buildings with an average wall thickness of 20 cm. Intensity parameter: momentum flux.

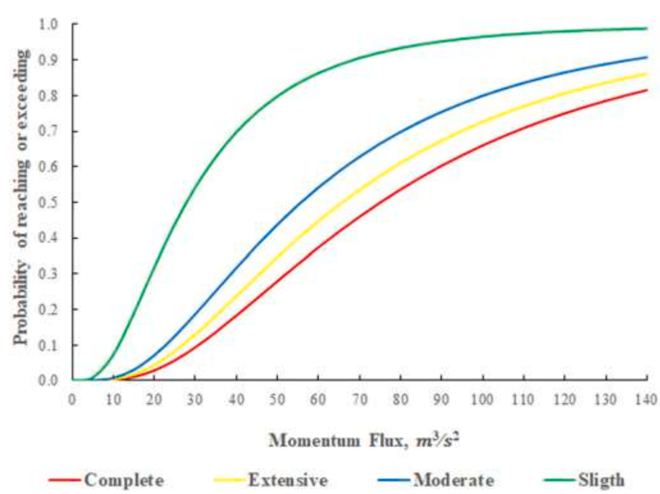

Fig. A13. Fragility curve for 3-storey CM buildings with an average wall thickness of 12 cm. Intensity parameter: momentum flux.

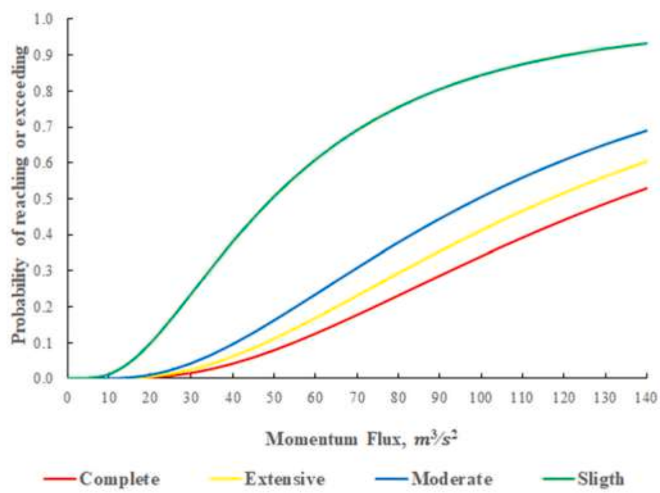

Fig. A14. Fragility curve for 3-storey CM buildings with an average wall thickness of 20 cm. Intensity parameter: momentum flux.

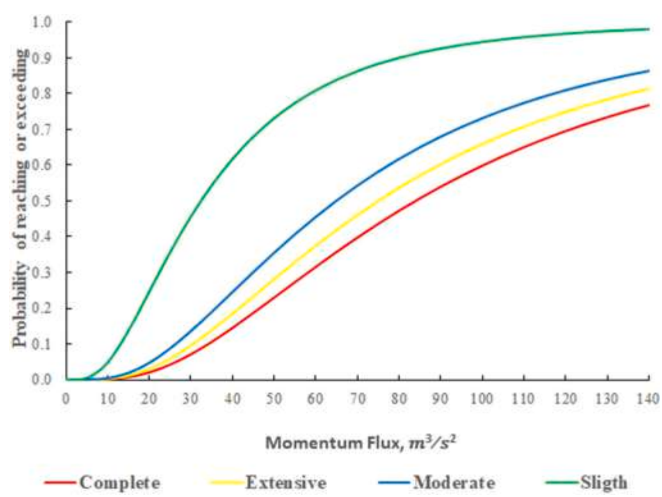

Fig. A15. Fragility curve for 4-storey CM buildings with an average wall thickness of 12 cm. Intensity parameter: momentum flux**.**

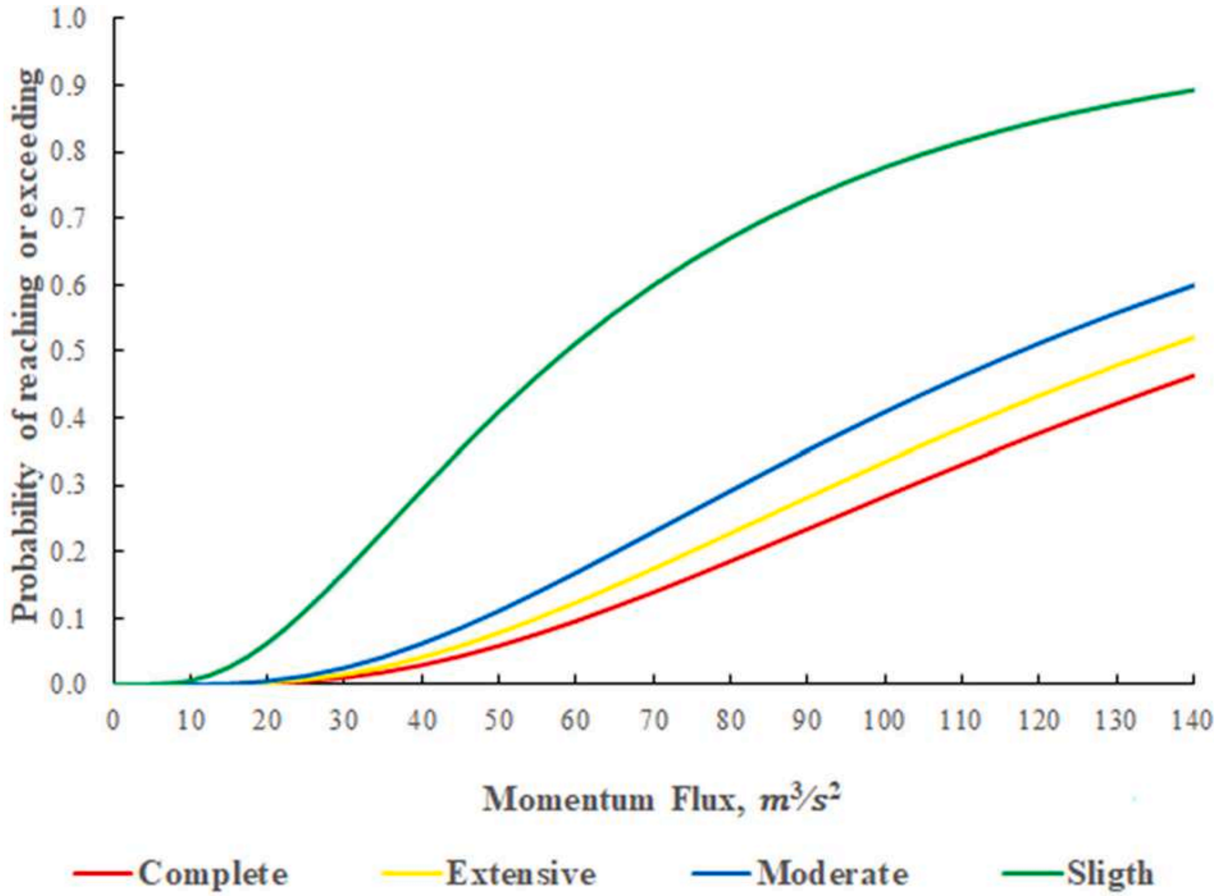

Fig. A16. Fragility curve for 4-storey CM buildings with an average wall thickness of 20 cm. Intensity parameter: momentum flux.

Appendix B. Appendix

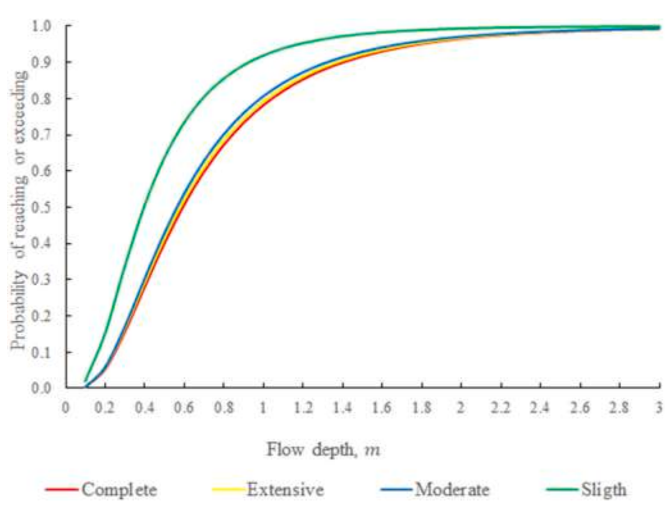

Fig. B1. Fragility curve for 1-storey URM buildings with an average wall thickness of 12 cm. Intensity parameter: flow depth.

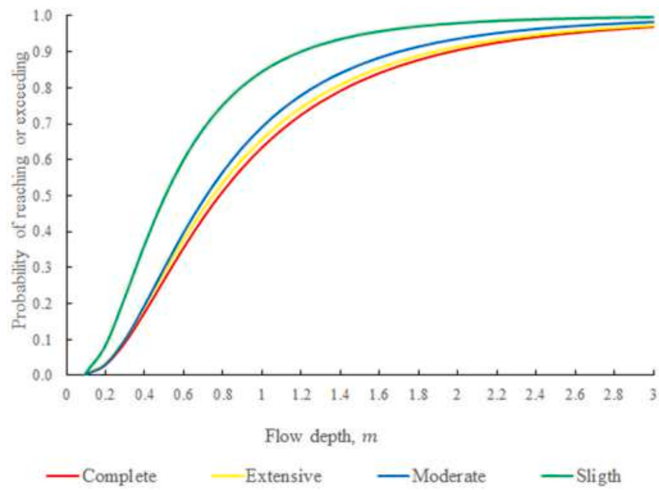

Fig. B2. Fragility curve for 1-storey URM buildings with an average wall thickness of 20 cm. Intensity parameter: flow depth.

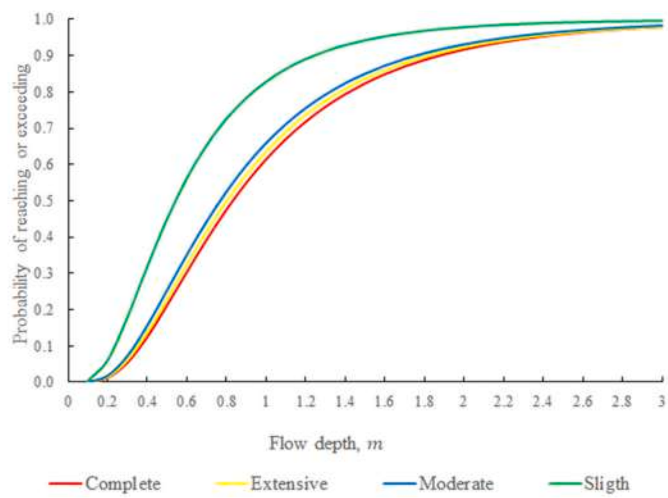

Fig. B3. Fragility curve for 2-storey URM buildings with an average wall thickness of 12 cm. Intensity parameter: flow depth.

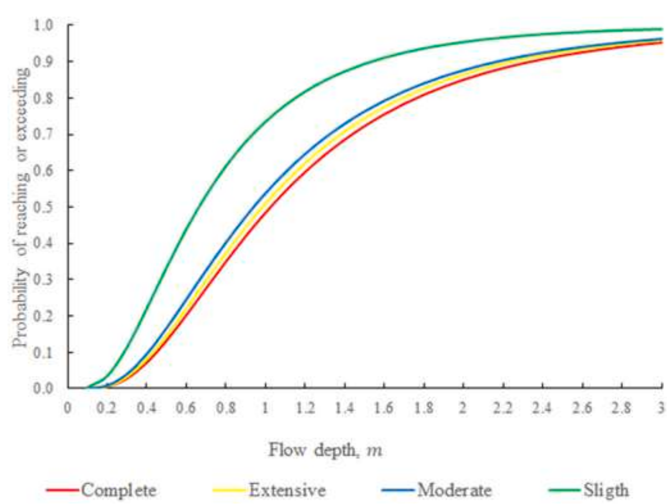

Fig. B4. Fragility curve for 2-storey URM buildings with an average wall thickness of 20 cm. Intensity parameter: flow depth.

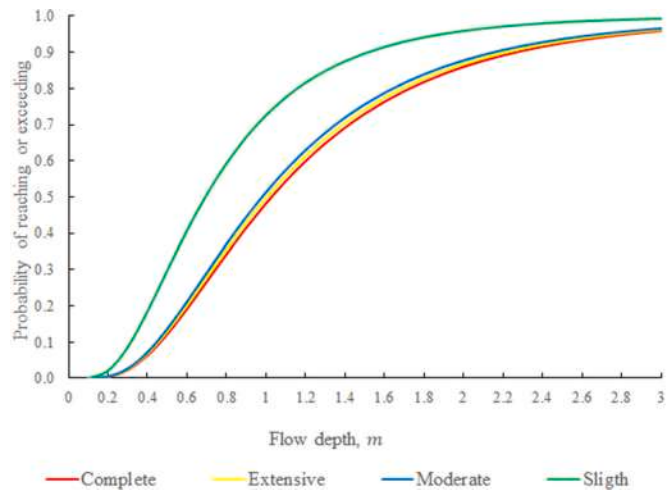

Fig. B5. Fragility curve for 3-storey URM buildings with an average wall thickness of 12 cm. Intensity parameter: flow depth.

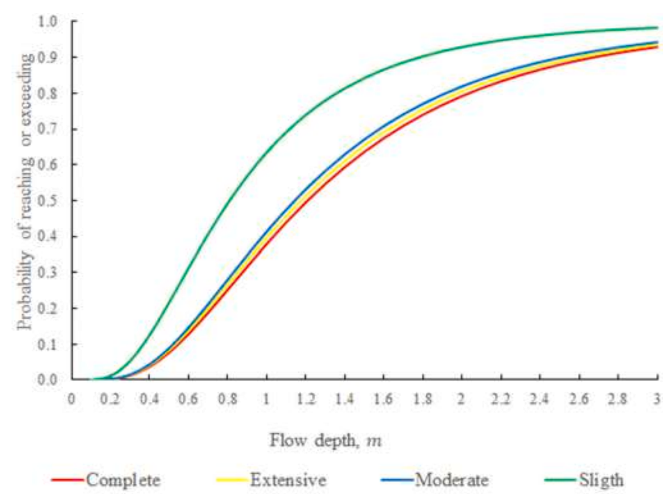

Fig. B6. Fragility curve for 3-storey URM buildings with an average wall thickness of 20 cm. Intensity parameter: flow depth.

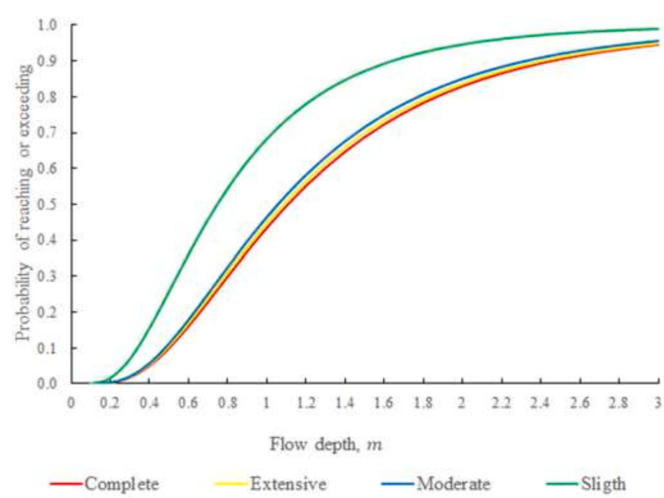

Fig. B7. Fragility curve for 4-storey URM buildings with an average wall thickness of 12 cm. Intensity parameter: flow depth.

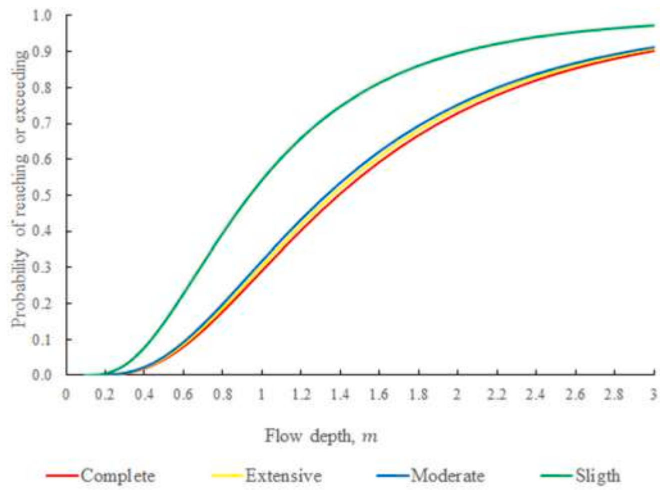

Fig. B8. Fragility curve for 4-storey URM buildings with an average wall thickness of 20 cm. Intensity parameter: flow depth.

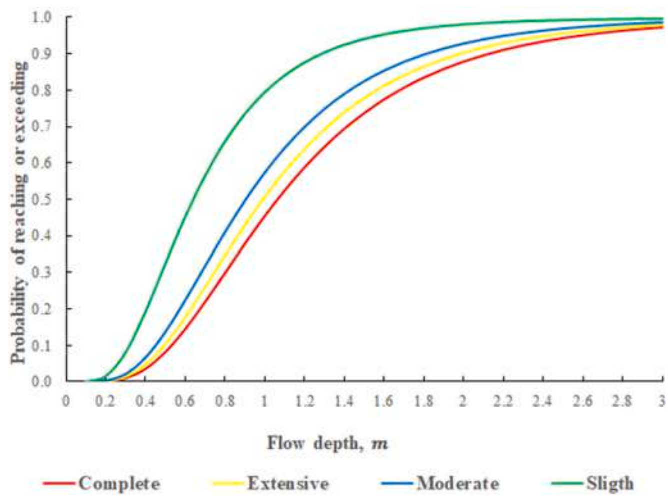

Fig. B9. Fragility curve for 1-storey CM buildings with an average wall thickness of 12 cm. Intensity parameter: flow depth.

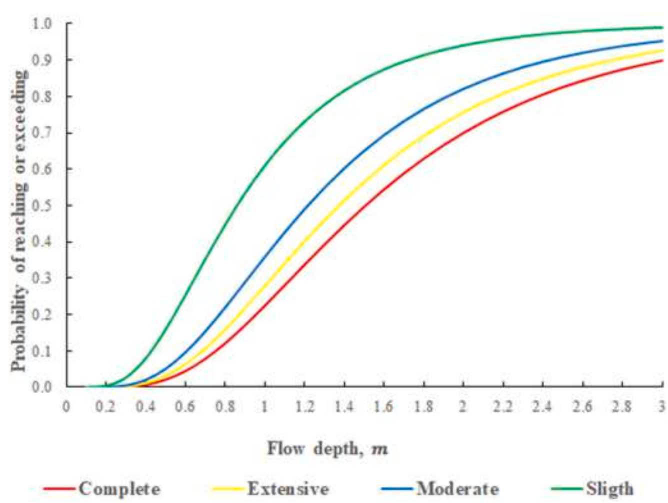

Fig. B10. Fragility curve for 1-storey CM buildings with an average wall thickness of 20 cm. Intensity parameter: flow depth.

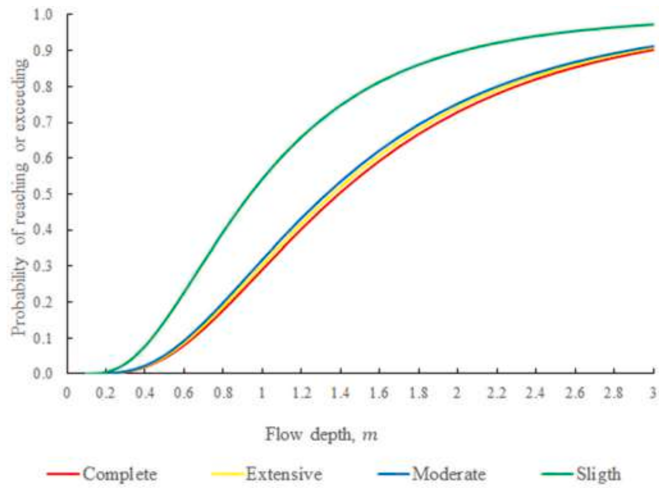

Fig. B11. Fragility curve for 2-storey CM buildings with an average wall thickness of 12 cm. Intensity parameter: flow depth.

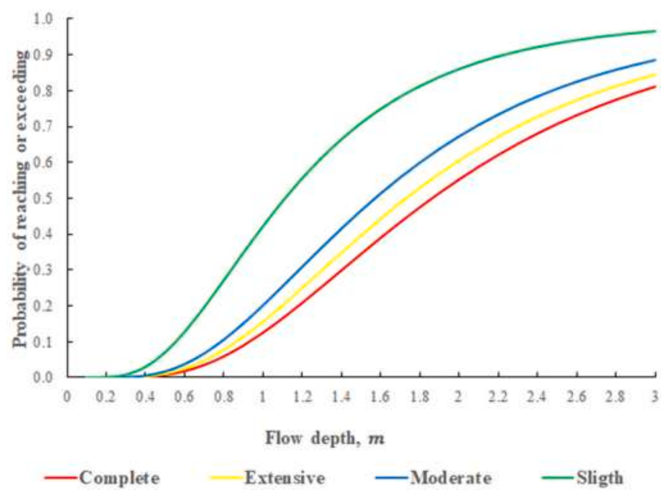

Fig. B12. Fragility curve for 2-storey CM buildings with an average wall thickness of 20 cm. Intensity parameter: flow depth.

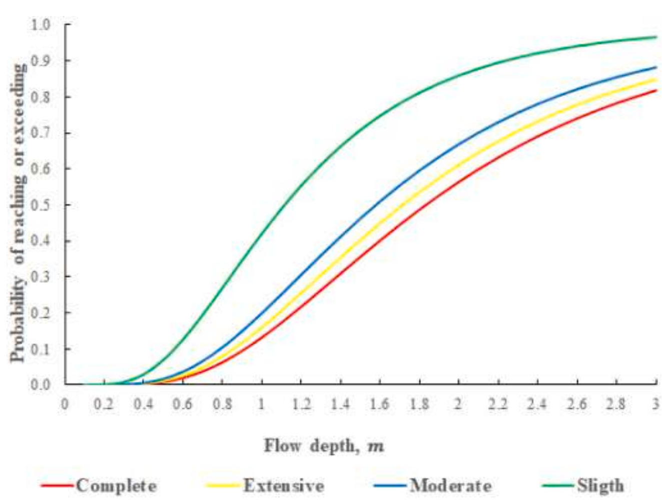

Fig. B13. Fragility curve for 3-storey CM buildings with an average wall thickness of 12 cm. Intensity parameter: flow depth.

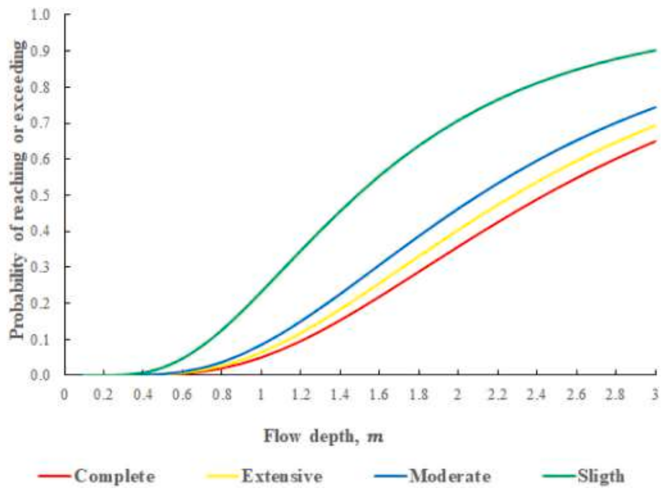

Fig. B14. Fragility curve for 3-storey CM buildings with an average wall thickness of 20 cm. Intensity parameter: flow depth.

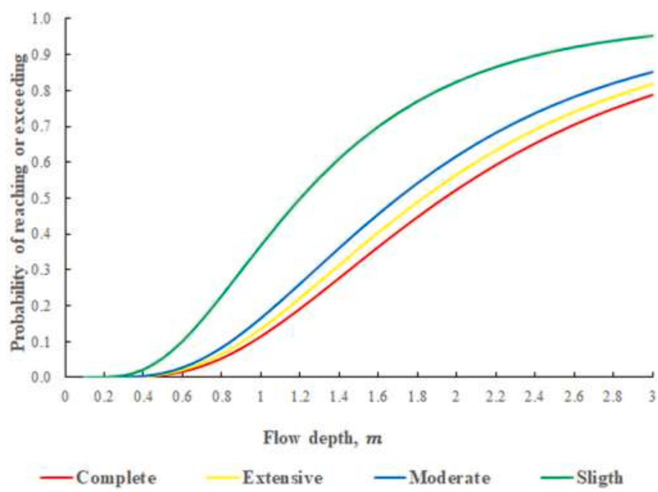

Fig. B15. Fragility curve for 4-storey CM buildings with an average wall thickness of 12 cm. Intensity parameter: flow depth.

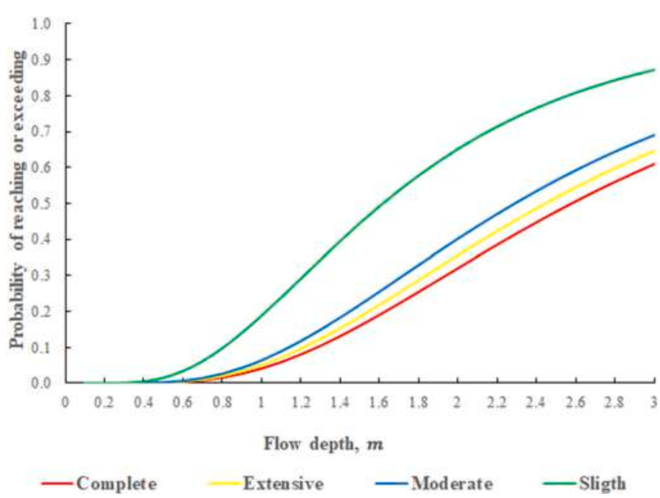

Fig. B16. Fragility curve for 4-storey CM buildings with an average wall thickness of 20 cm. Intensity parameter: flow depth.

Data availability

Data is available on reasonable request to the corresponding author.

References

Acevedo, A.B., Jaramillo, J.D., Yepes, C., Silva, V., Osorio, F.A., Villar, M., 2017. Evaluation of the seismic risk of the unreinforced masonry building stock in Antioquia, Colombia. Nat. Hazards 86 (S1), 31–54. https://doi.org/10.1007/s11069-016-2647-8.

Adhikari, R.K., D'Ayala, D., Fernandez, R., Yamin, L., Nassirpour, A., P Vatteri, A., Ferreira, C., Cortes, F., 2023. GLOSI taxonomy: a tool for 'seismic risk assessment' oriented classification of school buildings. Int. J. Disaster Risk Reduct. 87, 103594. https://doi.org/10.1016/j.ijdrr.2023.103594.

Afanador-García, N., Guerrero-Gómez, Gustavo Monroy-Sepúlveda, R., 2012. Mechanical & physical properties of solid, masonry ceramic bricks. Ciencia e Ingeniería Neogranadina 22 (1), 43–58. https://doi.org/10.18359/rcin.248.

Ahmed, A., Shahzada, K., Ali, S.M., Khan, A.N., Shah, S.A.A., 2019. Confined and unreinforced masonry structures in seismic areas: validation of macro models and cost analysis. Eng. Struct. 199 (8), 1–15. https://doi.org/10.1016/j.engstruct.2019.109612.

Alcocer-Martínez de Castro, S., Hernández-Barrios, H., Sandoval, R., H., 2013. Lateral strength envelope for confined masonry structures. Revista de Ingeniería Sísmica 54 (89), 24–54. https://doi.org/10.18867/ris.89.163.

Aristizábal, E., Sánchez, O., 2020. Spatial and temporal patterns and the socioeconomic impacts of landslides in the tropical and mountainous Colombian Andes. Disasters 44 (3), 596–618. https://doi.org/10.1111/disa.12391.

Armanini, A., 2008. On the dynamic impact of debris flows. In: Armanini, A., Michiue, M. (Eds.), Recent Developments on Debris Flows, 1st ed, Lecture Notes in Earth Sciences. Springer, pp. 208–226. https://doi.org/10.1007/bfb0117770.

Asteris, P.G., Chronopoulos, M.P., Chrysostomou, C.Z., Varum, H., Plevris, V., Kyriakides, N., Silva, V., 2014. Seismic vulnerability assessment of historical masonry structural systems. Eng. Struct. 62–63, 118–134. https://doi.org/10.1016/j.engstruct.2014.01.031.

Bell, R., Glade, T., 2004. Quantitative risk analysis for landslides – examples from Bíldudalur, NW-Iceland. Nat. Hazards Earth Syst. Sci. 4 (1), 117–131. https://doi.org/10.5194/nhess-4-117-2004.

Borah, B., Kaushik, H.B., Singhal, V., 2023. Analysis and design of confined masonry structures: review and future research directions. Buildings 13 (5). https://doi.org/10.3390/buildings13051282.

Cabral, V., Reis, F., Veloso, V., Ogura, A., Zarfl, C., 2023. A multi-step hazard assessment for debris-flow prone areas influenced by hydroclimatic events. Eng. Geol. 313 (106961). https://doi.org/10.1016/j.enggeo.2022.106961.

Capparelli, G., Liguori, F.S., Madeo, A., Versace, P., 2023. A rapid numerical-based vulnerability assessment method for masonry buildings subject to flood. Int. J. Disaster Risk Reduct. 97 (104001). https://doi.org/10.1016/j.ijdrr.2023.104001.

CEN, 2005. Eurocode 6 - Design of masonry structures - part 1-1: general rules for reinforced and unreinforced masonry structures. European Committee for Standardization. https://www.phd.eng.br/wp-content/uploads/2015/02/en.1996.1.1.2005.pdf.

Chen, H., Lee, C.F., 2004. Geohazards of slope mass movement and its prevention in Hong Kong. Eng. Geol. 76 (1–2), 3–25. https://doi.org/10.1016/j.enggeo.2004.06.003.

Chen, J., Yang, J., Li, J., 2016. A GF- discrepancy for point selection in stochastic seismic response analysis of structures with uncertain parameters. Struct. Saf. 59, 20–31. https://doi.org/10.1016/j.strusafe.2015.11.001.

Chen, M., Tang, C., Zhang, X., Xiong, J., Chang, M., Shi, Q., Wang, F., Li, M., 2021. Quantitative assessment of physical fragility of buildings to the debris flow on 20 August 2019 in the Cutou gully, Wenchuan, southwestern China. Eng. Geol. 293 (106319). https://doi.org/10.1016/j.enggeo.2021.106319.

Chen, M., Luo, Y., Tang, C., Li, N., 2023. Quantitative assessment of expected direct economic losses of buildings for debris flows in multiple rainfall intensity scenarios in Yangling Gully, Southwest China. Nat. Hazards 120, 2993–3014. https://doi.org/10.1007/s11069-023-06315-0.

Cheung, A.K.C., Yiu, J., Lam, H.W.K., Sze, E.H.Y., 2018. Advanced numerical analysis of landslide debris mobility and barrier interaction. HKIE Trans. Hong Kong Inst. Eng. 25 (2), 76–89. https://doi.org/10.1080/1023697X.2018.1462106.

Corominas, J., van Westen, C., Frattini, P., Cascini, L., Malet, J.P., Fotopoulou, S., Catani, F., Van Den Eeckhaut, M., Mavrouli, O., Agliardi, F., Pitilakis, K., Winter, M. G., Pastor, M., Ferlisi, S., Tofani, V., Hervás, J., Smith, J.T., 2014. Recommendations for the quantitative analysis of landslide risk. Bull. Eng. Geol. Environ. 73 (2), 209–263. https://doi.org/10.1007/s10064-013-0538-8.

Cruden, D.M., 1991. A simple definition of a landslide. Bull. Int. Assoc. Eng. Geol. 43 (1), 27–29. https://doi.org/10.1007/BF02590167.

DAPARD, 2015. Informe de asesoría o asistencia técnica. Municipio Salgar. Gobernación de Antioquia.

Du, J., Yin, K., Nadim, F., Lacasse, S., 2013. Quantitative vulnerability estimation for individual landslides. In: 18th International Conference on Soil Mechanics and Geotechnical Engineering: Challenges and Innovations in Geotechnics, ICSMGE 2013, pp. 2181–2184. https://www.issmge.org/publications/publication/quantitative-vulnerability-estimation-for-individual-landslides.

EERI Committee, 1986. Glossary of terms for probabilistic seismic-risk and hazard analysis. Bull. N. Z. Soc. Earthq. Eng. 19 (3), 155–157. https://doi.org/10.5459/bnzsee.19.3.155-157.

Eidsvig, U.M.K., Papathoma-Köhle, M., Du, J., Glade, T., Vangelsten, B.V., 2014. Quantification of model uncertainty in debris flow vulnerability assessment. Eng. Geol. 181, 15–26. https://doi.org/10.1016/j.enggeo.2014.08.006.

Elghazouli, A.Y., Peppin, R.J., 2011. Seismic design of buildings to eurocode 8. Noise Control Eng. J. 59 (2). https://doi.org/10.3397/1.3532782, 212-212,1.

Fang, Q., Liu, S., Zhong, G., Zhang, H., Liang, J., Zhen, Y., 2021. Nonlinear simulation and vulnerability analysis of masonry structures impacted by flash floods. Shock. Vib. 2021, 1–20. https://doi.org/10.1155/2021/6682234.

FEMA, 2003. HAZUS-MH MR4. Technical manual. National Institute of Building Sciences and Federal Emergency Management Agency (NIBS and FEMA).

FEMA, 2012. Hazus–MH 2.1. Technical manual. Federal Emergency Management Agency. https://www.researchgate.net/publication/328175418_HAZUS-MH_21_Earthquake_Model_Technical_Manual.

FEMA, 2017. Hazus Tsunami model technical guidance, 11. https://www.fema.gov/flood-maps/products-tools/hazus.

FEMA P-58, 2012. Seismic performance assessment of buildings, 2nd ed. 1. FEMA, p. 9 https://www.atcouncil.org/docman/fema/246-fema-p-58-1-seismic-performance-assessment-of-buildings-volume-1-methodology-second-edition/file.

Feng, S.J., Gao, H.Y., Chen, H.X., 2019. Numerical simulation of failure process of buildings under the impact of flow slide. Environ. Sci. Eng. 2, 217–223. https://doi.org/10.1007/978-981-13-2224-2_27.

Fenton, V.C., 1989. Seismic design of masonry. Ann. N. Y. Acad. Sci. 558 (1), 288–299. https://doi.org/10.1111/j.1749-6632.1989.tb22578.x.

Flores, L.E., Alcocer, S.M., 1996. Calculated response of confined masonry structures. In: Eleventh World Conference on Earthquake Engineering, Acapulco, Paper No. 1830.

Flores, V., Sánchez-Tizapa, S., Arroyo, R., Barragán, R., 2013. Mechanical properties of solid clay brick masonry used in Chilpancingo, Gro (Mexico). Inform. Constr. 65 (531), 387–395. https://doi.org/10.3989/ic.12.084.

Fuchs, S., Heiss, K., Hübl, J., 2007. Towards an empirical vulnerability function for use in debris flow risk assessment. Nat. Hazards Earth Syst. Sci. 7 (5), 495–506. https://doi.org/10.5194/nhess-7-495-2007.

Fuchs, S., Heiser, M., Schlögl, M., Zischg, A., Papathoma-Köhle, M., Keiler, M., 2019a. Short communication: a model to predict flood loss in mountain areas. Environ. Model. Softw. 117, 176–180. https://doi.org/10.1016/j.envsoft.2019.03.026.

Fuchs, S., Keiler, M., Ortlepp, R., Schinke, R., Papathoma-Köhle, M., 2019b. Recent advances in vulnerability assessment for the built environment exposed to torrential hazards: challenges and the way forward. J. Hydrol. 575, 587–595. https://doi.org/10.1016/j.jhydrol.2019.05.067.

Gonen, S., Pulatsu, B., Erdogmus, E., Lourenço, P.B., Soyoz, S., 2022. Effects of spatial variability and correlation in stochastic discontinuum analysis of unreinforced masonry walls. Constr. Build. Mater. 337 (127511), 1–39. https://doi.org/10.1016/j.conbuildmat.2022.127511.

Gonzales, G., Aguilar, A., Huaco, G., 2020. Incremental dynamic analysis of a 60 year old hospital with handmade brick masonry walls. In: 18th LACCEI International Multi-Conference for Engineering, Education, and Technology, pp. 1–6. https://doi.org/10.18687/LACCEI2020.1.1.375.

Gumaste, K.S., Rao, K.S.N., Reddy, B.V.V., Jagadish, K.S., 2007. Strength and elasticity of brick masonry prisms and wallettes under compression. Mater. Struct. 40 (2), 241–253. https://doi.org/10.1617/s11527-006-9141-9.

Haugen, E., Kaynia, A., 2008. Vulnerability of structures impacted by debris flow. In: Landslides and Engineered Slopes. From the Past to the Future, pp. 381–387. https://doi.org/10.1201/9780203885284-c37.

Heijungs, R., 2020. On the number of Monte Carlo runs in comparative probabilistic LCA. Int. J. Life Cycle Assess. 25 (2), 394–402. https://doi.org/10.1007/s11367-019-01698-4.

Highland, L.M., Bobrowsky, P., 2008. The landslide Handbook - A guide to understanding landslides. In: U.S. Geological Survey Circular, p. 129. https://doi.org/10.3133/cir1325.

Hu, K., Wei, F., Li, Y., 2011. Real-time measurement and preliminary analysis of debris-flow impact force at Jiangjia Ravine, China. Earth Surf. Process. Landf. 36 (9), 1268–1278. https://doi.org/10.1002/esp.2155.

Hu, K.H., Cui, P., Zhang, J.Q., 2012. Characteristics of damage to buildings by debris flows on 7 August 2010 in Zhouqu, Western China. Nat. Hazards Earth Syst. Sci. 12 (7), 2209–2217. https://doi.org/10.5194/nhess-12-2209-2012.

Huang, X., Zhang, Z., Xiang, G., 2023a. Sensitivity analysis of a built environment exposed to the synthetic monophasic viscous debris flow impacts with 3-D numerical simulations. Nat. Hazards Earth Syst. Sci. 23 (2), 871–889. https://doi.org/10.5194/nhess-23-871-2023.

Huang, Y., Zhang, J., Zhang, L., Ming, Z., He, H., Chen, R., Ge, Y., Liu, R., 2023b. How spatial resolution of remote sensing image affects earthquake triggered landslide detection: an example from 2022 luding earthquake, Sichuan, China. Land 12 (3). https://doi.org/10.3390/land12030681.

Huebl, J., Nagl, G., Suda, J., Rudolf-Miklau, F., 2017. Standardized stress model for design of torrential barriers under impact by debris flow (according to Austrian Standard Regulation 24801). Int. J. Eros. Control Eng. 10 (1), 47–55. https://doi.org/10.13101/ijece.10.47.

Hungr, O., Leroueil, S., Picarelli, L., 2014. The Varnes classification of landslide types, an update. Landslides 11 (2), 167–194. https://doi.org/10.1007/s10346-013-0436-y.

Jafari, S., Rots, J.G., Esposito, R., Messali, F., 2017. Characterizing the material properties of Dutch unreinforced masonry. Procedia Eng. 193, 250–257. https://doi.org/10.1016/j.proeng.2017.06.211.

Jafari, S., Rots, J.G., Esposito, R., 2022. A correlation study to support material characterisation of typical Dutch masonry structures. J. Build. Eng. 45, 103450. https://doi.org/10.1016/j.jobe.2021.103450.

Jakob, M., Stein, D., Ulmi, M., 2012. Vulnerability of buildings to debris flow impact. Nat. Hazards 60, 241–261. https://doi.org/10.1007/s11069-011-0007-2.

Joshi, D.A., Jain, R.K., 2013. Evaluation of compressive strength and basic compressive stress of clay brick unreinforced masonry by prism test. Int. J. Sci. Res. 4 (5), 2319–7064. https://www.ijsr.net/archive/v4i5/SUB154258.pdf.
Kang, H., Kim, Y., 2016. The physical vulnerability of different types of building structure to debris flow events. Nat. Hazards 80, 1475–1493. https://doi.org/10.1007/s11069-015-2032-z.
Kean, J.W., Staley, D.M., Lancaster, J.T., Rengers, F.K., Swanson, B.J., Coe, J.A., Hernandez, J.L., Sigman, A.J., Allstadt, K.E., Lindsay, D.N., 2019. Inundation, flow dynamics, and damage in the 9 January 2018 Montecito debris-flow event, California, USA: opportunities and challenges for post-wildfire risk assessment. Geosphere 15 (4), 1140–1163. https://doi.org/10.1130/GES02048.1.
Khan, M.A., 2013. Seismic design for buildings. In: In Earthquake-Resistant Structures. Butterworth-Heinemann, pp. 283–315. https://doi.org/10.1016/b978-1-85617-501-2.00010-9.
Khanmohammadi, M., Behnam, H., Marefat, M.S., 2014. Seismic behaviour prediction of flanged unreinforced masonry (FURM) walls. J. Earthq. Eng. 18 (5), 759–784. https://doi.org/10.1080/13632469.2014.897273.
Li, Z., Nadim, F., Huang, H., Uzielli, M., Lacasse, S., 2010. Quantitative vulnerability estimation for scenario-based landslide hazards. Landslides 7 (2), 125–134. https://doi.org/10.1007/s10346-009-0190-3.
Liang, Y., Xiong, F., 2019. Quantification of debris flow vulnerability of typical bridge substructure based on impact force simulation. Geomat. Nat. Haz. Risk 10 (1), 1839–1862. https://doi.org/10.1080/19475705.2019.1641564.
Liu, X., Lei, J., 2003. A method for assessing regional debris flow risk: an application in Zhaotong of Yunnan province (SW China). Geomorphology 52 (3–4), 181–191. https://doi.org/10.1016/S0169-555X(02)00242-8.
Liu, X., Yue, Z.Q., Tham, L.G., Lee, C.F., 2002. Empirical assessment of debris flow risk on a regional scale in Yunnan province, Southwestern China. Environ. Manag. 30 (2), 249–264. https://doi.org/10.1007/s00267-001-2658-3.
Luo, H.Y., Shen, P., Zhang, L.M., 2019a. How does a cluster of buildings affect landslide mobility: a case study of the Shenzhen landslide. Landslides 16 (12), 2421–2431. https://doi.org/10.1007/s10346-019-01239-y.
Luo, H.Y., Zhang, L.L., Zhang, L.M., 2019b. Progressive failure of buildings under landslide impact. Landslides 16, 1327–1340. https://doi.org/10.1007/s10346-019-01164-0.
Luo, H.Y., Fan, R.L., Wang, H.J., Zhang, L.M., 2020. Physics of building vulnerability to debris flows, floods and earth flows. Eng. Geol. 271, 1–13. https://doi.org/10.1016/j.enggeo.2020.105611.
Luo, H., Zhang, L.M., He, J., Yin, K., 2021. Reliability based formulation of building vulnerability to debris flow impacts. Can. Geotech. J. 59 (1), 1–49. https://doi.org/10.1139/cgj-2020-0120.
Luo, H.Y., Zhang, L.M., Zhang, L.L., He, J., Yin, K.S., 2023. Vulnerability of buildings to landslides: the state of the art and future needs. Earth Sci. Rev. 238 (10), 104329. https://doi.org/10.1016/j.earscirev.2023.104329.
Magenes, G., Calvi, G.M., 1997. In-plane seismic response of brick masonry walls. Earthq. Eng. Struct. Dyn. 26 (11), 1091–1112. https://doi.org/10.1002/(SICI)1096-9845(199711)26:11<1091::AID-EQE693>3.0.CO;2-6.
Mann, W., Müller, H., 1982. Failure of shear-stressed masonry - an enlarged theory, tests and application to shear walls. Proc. Br. Ceram. Soc. 223–235.
Masonry Standards Joint Committee, 2013. TMS 402/602–16. Building code requirements and specification for masonry structures. The Masonry Society. https://masonrysociety.org/product/tms-402-602-2016/.
Mavrouli, O., Corominas, J., 2010. Rockfall vulnerability assessment for reinforced concrete buildings. Nat. Hazards Earth Syst. Sci. 10 (10), 2055–2066. https://doi.org/10.5194/nhess-10-2055-2010.
Mavrouli, O., Fotopoulou, S., Pitilakis, K., Zuccaro, G., Corominas, J., Santo, A., Cacace, F., De Gregorio, D., Di Crescenzo, G., Foerster, E., Ulrich, T., 2014. Vulnerability assessment for reinforced concrete buildings exposed to landslides. Bull. Eng. Geol. Environ. 73, 265–289. https://doi.org/10.1007/s10064-014-0573-0.
Mazzorana, B., Simoni, S., Scherer, C., Gems, B., Fuchs, S., Keiler, M., 2014. A physical approach on flood risk vulnerability of buildings. Hydrol. Earth Syst. Sci. 18 (9), 3817–3836. https://doi.org/10.5194/hess-18-3817-2014.
Meli, R., Reyes, A., 1971. Mechanical Properties of Masonry. Instituto de Ingeniería, Universidad Nacional Autónoma de México http://132.248.9.195/SerieAzul/288.pdf.
Michael-Leiba, M., Baynes, F., Scott, G., Granger, K., 2012. Quantitative landslide risk assessment of Cairns, Australia. In: Landslide Hazard and Risk, pp. 621–642. https://doi.org/10.1002/9780470012659.ch21.
Muhit, I.B., Masia, M.J., Stewart, M.G., Isfeld, A.C., 2022. Spatial variability and stochastic finite element model of unreinforced masonry veneer wall system under Out-of-plane loading. Eng. Struct. 267, 114674. https://doi.org/10.1016/j.engstruct.2022.114674.
Odacıoğlu, O.G., Doğan, O., 2019. An experimental study to determine sliding shear strength and internal frictional coefficient of clay brick wall in a masonry building. Uluslararası Muhendislik Arastirma ve Gelistirme Dergisi 11 (2), 670–676. https://doi.org/10.29137/umagd.545396.
Panyakapo, P., 2014. Cyclic Pushover Analysis procedure to estimate seismic demands for buildings. Eng. Struct. 66, 10–23. https://doi.org/10.1016/j.engstruct.2014.02.001.
Papathoma-Köhle, M., Kappes, M., Keiler, M., Glade, T., 2011. Physical vulnerability assessment for alpine hazards: state of the art and future needs. Nat. Hazards 58 (2), 645–680. https://doi.org/10.1007/s11069-010-9632-4.
Papathoma-Köhle, M., Ulbrich, T., Keiler, M., Pedoth, L., Totschnig, R., Glade, T., Schneiderbauer, S., Eidswig, U., 2014. Vulnerability to heat waves, floods, and landslides in mountainous terrain: Test cases in South Tyrol. In: Assessment of Vulnerability to Natural Hazards: A European Perspective, pp. 179–201. https://doi.org/10.1016/B978-0-12-410528-7.00008-4.
Papathoma-Köhle, M., Gems, B., Sturm, M., Fuchs, S., 2017. Matrices, curves and indicators: a review of approaches to assess physical vulnerability to debris flows. Earth Sci. Rev. 171, 272–288. https://doi.org/10.1016/j.earscirev.2017.06.007.
Papathoma-Köhle, M., Schlögl, M., Fuchs, S., 2019. Vulnerability indicators for natural hazards: an innovative selection and weighting approach. Sci. Rep. 9 (1). https://doi.org/10.1038/s41598-019-50257-2.
Papathoma-Köhle, M., Schlögl, M., Dosser, L., Roesch, F., Borga, M., Erlicher, M., Keiler, M., Fuchs, S., 2022. Physical vulnerability to dynamic flooding: vulnerability curves and vulnerability indices. J. Hydrol. 607 (127501), 1–11. https://doi.org/10.1016/j.jhydrol.2022.127501.
Parisi, F., Sabella, G., 2017. Flow-type landslide fragility of reinforced concrete framed buildings. Eng. Struct. 131, 28–43. https://doi.org/10.1016/j.engstruct.2016.10.013.
Paulay, T., Priestley, M.J.N., 1992. Seismic design of reinforced concrete and masonry buildings. Bull. N. Z. Soc. Earthq. Eng. 25 (4), 362. https://doi.org/10.5459/bnzsee.25.4.362.
Prieto, J.A., Journeay, M., Acevedo, A.B., Arbelaez, J.D., Ulmi, M., 2018a. Development of structural debris flow fragility curves (debris flow buildings resistance) using momentum flux rate as a hazard parameter. Eng. Geol. 239, 144–157. https://doi.org/10.1016/j.enggeo.2018.03.014.
Prieto, J.A., Journeay, M., Acevedo, A.B., Arbelaez, J.D., Ulmi, M., 2018b. Development of structural debris flow fragility curves (debris flow buildings resistance) using momentum flux rate as a hazard parameter. Eng. Geol. 239, 144–157. https://doi.org/10.1016/j.enggeo.2018.03.014.
Pu, J., Huang, Y., Guo, Z., Bi, Y., Xu, C., Li, X., Chen, Z., 2023. Physical vulnerability of reinforced concrete buildings under debris avalanche impact based on GF-discrepancy and DEM-FEM. Nat. Hazards 120 (2024), 2571–2597. https://doi.org/10.1007/s11069-023-06294-2.
Pulatsu, B., Gonen, S., Erdogmus, E., Lourenço, P.B., Lemos, J.V., Hazzard, J., 2020. Tensile fracture mechanism of masonry wallettes parallel to bed joints: a stochastic discontinuum analysi. Modelling—Int. Open Access J. Model. Eng. Sci. 1 (2), 78–93. https://doi.org/10.3390/modelling1020006.
Quan Luna, B., Blahut, J., Van Westen, C.J., Sterlacchini, S., Van Asch, T.W.J., Akbas, S. O., 2011. The application of numerical debris flow modelling for the generation of physical vulnerability curves. Nat. Hazards Earth Syst. Sci. 11 (7), 2047–2060. https://doi.org/10.5194/nhess-11-2047-2011.
Ramos Cañón, A.M., Reyes Merchán, A.A., Munévar Peña, M.A., Ruiz Peña, G.L., Machuca Castellanos, S.V., Rangel Flórez, M.S., Prada Sarmiento, L.F., Cabrera, M.Á., Rodríguez Pineda, C.E., Escobar Castañeda, N., Quintero Ortiz, C.A., Escobar Vargas, J.A., Giraldo Osorio, J.D., Medina Orjuela, M.S., Durán Santana, L., Trujillo Osorio, D.E., Medina Ávila, D.F., Capachero Martínez, C.A., León Delgado, D., Pérez Moreno, M.A., 2021. Methodological guide for torrential flood hazard zoning, 1st ed. Colombian Geological Service and the Pontifical Javierian University. https://doi.org/10.32685/9789585313156.
Rosenblueth, E., 1975. Point estimates for probability moments. Proc. Natl. Acad. Sci. USA 72 (10), 3812–3814. https://doi.org/10.1073/pnas.72.10.3812.
Santi, P.M., Hewitt, K., VanDine, D.F., Cruz, E.B., 2011. Debris-flow impact, vulnerability, and response. Nat. Hazards 56 (1), 371–402. https://doi.org/10.1007/s11069-010-9576-8.
Sterlacchini, S., Frigerio, S., Giacomelli, P., Brambilla, M., 2007. Landslide risk analysis: a multi-disciplinary methodological approach. Nat. Hazards Earth Syst. Sci. 7 (6), 657–675. https://doi.org/10.5194/nhess-7-657-2007.
Sturm, M., Gems, B., Keller, F., Mazzorana, B., Fuchs, S., Papathoma-Köhle, M., Aufleger, M., 2018a. Experimental analyses of impact forces on buildings exposed to fluvial hazards. J. Hydrol. 565, 1029–1042. https://doi.org/10.1016/j.jhydrol.2018.07.070.
Sturm, M., Gems, B., Keller, F., Mazzorana, B., Fuchs, S., Papathoma-Köhle, M., Aufleger, M., 2018b. Understanding impact dynamics on buildings caused by fluviatile sediment transport. Geomorphology 321 (4), 147–157. https://doi.org/10.1016/j.geomorph.2018.08.016.
Szabó, S., Funari, M.F., Lourenço, P.B., 2023. Masonry patterns' influence on the damage assessment of URM walls: current and future trends. Dev. Built Environ. 13, 100119. https://doi.org/10.1016/j.dibe.2023.100119.
Thinley, K., Hao, H., 2017. Seismic performance of reinforced concrete frame buildings in Bhutan based on fuzzy probability analysis. Soil Dyn. Earthq. Eng. 92, 604–620. https://doi.org/10.1016/j.soildyn.2016.11.004.
Thouret, J.C., Antoine, S., Magill, C., Ollier, C., 2020. Lahars and debris flows: characteristics and impacts. Earth Sci. Rev. 201 (4), 103003. https://doi.org/10.1016/j.earscirev.2019.103003.
Vagnon, F., Segalini, A., 2016. Debris flow impact estimation on a rigid barrier. Nat. Hazards Earth Syst. Sci. 16 (7), 1691–1697. https://doi.org/10.5194/nhess-16-1691-2016.

Vamvatsikos, D., Pantazopoulou, S.J., 2010. Simplified vulnerability assessment of historical city cores - The example of the city of Xanthi. In: 9th US National and 10th Canadian Conference on Earthquake Engineering 2010, Including Papers from the 4th International Tsunami Symposium, 7 (703), pp. 5674–5683. https://www.caee.ca/10CCEEpdf/2010EQConf-000703.pdf.

Villar-Vega, M., Silva, V., Crowley, H., Yepes, C., Tarque, N., Acevedo, A.B., Hube, M.A., Gustavo, C.D., María, H.S., 2017. Development of a fragility model for the residential building stock in South America. Earthquake Spectra 33 (2), 581–604. https://doi.org/10.1193/010716EQS005M.

Walhorn, E., Kölke, A., Hübner, B., Dinkler, D., 2005. Fluid-structure coupling within a monolithic model involving free surface flows. Comput. Struct. 83 (25–26), 2100–2111. https://doi.org/10.1016/j.compstruc.2005.03.010.

Yang, J., Tao, J., Sudret, B., Chen, J., 2020. Generalized F-discrepancy-based point selection strategy for dependent random variables in uncertainty quantification of nonlinear structures. Int. J. Numer. Methods Eng. 121 (7), 1507–1529. https://doi.org/10.1002/nme.6277.

Yekrangnia, M., 2023. Seismic vulnerability assessment of masonry residential buildings in the older parts of Tehran through fragility curves and basic RVS scores. Buildings 13 (2). https://doi.org/10.3390/buildings13020302.

Zeng, C., Cui, P., Su, Z., Lei, Y., Chen, R., 2015. Failure modes of reinforced concrete columns of buildings under debris flow impact. Landslides 12 (2015), 561–571. https://doi.org/10.1007/s10346-014-0490-0.

Zhang, S., Zhang, L., Li, X., Xu, Q., 2018. Physical vulnerability models for assessing building damage by debris flows. Eng. Geol. 247, 145–158. https://doi.org/10.1016/j.enggeo.2018.10.017.